US 20120003114A1

(19) **United States**

(12) **Patent Application Publication**

Baker et al.

(10) **Pub. No.: US 2012/0003114 A1**

(43) **Pub. Date: Jan. 5, 2012**

(54) **NANOSTRUCTURED MN-AL PERMANENT MAGNETS AND METHODS OF PRODUCING SAME**

(76) Inventors: **Ian Baker**, Etna, NH (US); **Qi Zeng**, Sinking Spring, PA (US)

(21) Appl. No.: **13/164,495**

(22) Filed: **Jun. 20, 2011**

Related U.S. Application Data

(63) Continuation-in-part of application No. 12/089,876, filed on Apr. 23, 2010, filed as application No. PCT/US06/41790 on Oct. 27, 2006.

(60) Provisional application No. 60/730,697, filed on Oct. 27, 2005.

Publication Classification

(51) **Int. Cl.**

B22F 1/00	(2006.01)
B22F 9/04	(2006.01)
B22F 3/02	(2006.01)

(52) **U.S. Cl.** **419/62**; 75/245

(57) **ABSTRACT**

A bulky consolidated nanostructured manganese aluminum alloy includes at least about 80% of a magnetic τ phase and having a macroscopic composition of MnXAlYDoZ, where Do is a dopant, X ranges from 52-58 atomic %, Y ranges from 42-48 atomic %, and Z ranges from 0 to 3 atomic %. A method for producing a bulky nanocrystalline solid is provided. The method includes melting a mixture of metals to form a substantially homogenous solution. The method also includes casting the solution to form ingots, measuring compositions of the ingots; crushing the ingots to form crushed powders, and milling the crushed powders to form nanocrystalline powders. The method further includes verifying the presence of τ phase and determining the amount of the τ phase, and simultaneously consolidating the nanocrystalline powders into a bulky nanocrystalline solid and undergoing phase transformation from ϵ phase to at least 80% τ phase, β and γ2 phases.

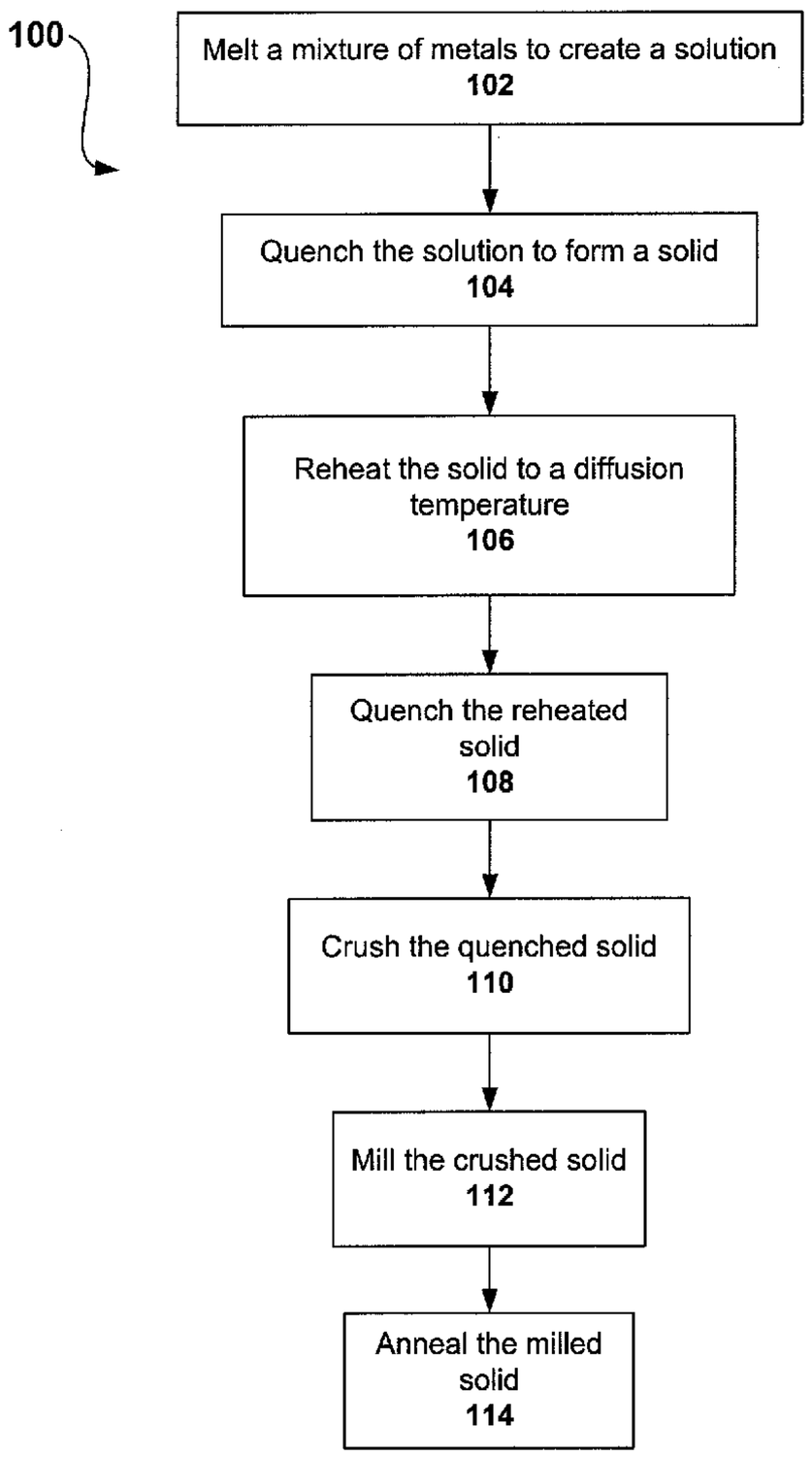

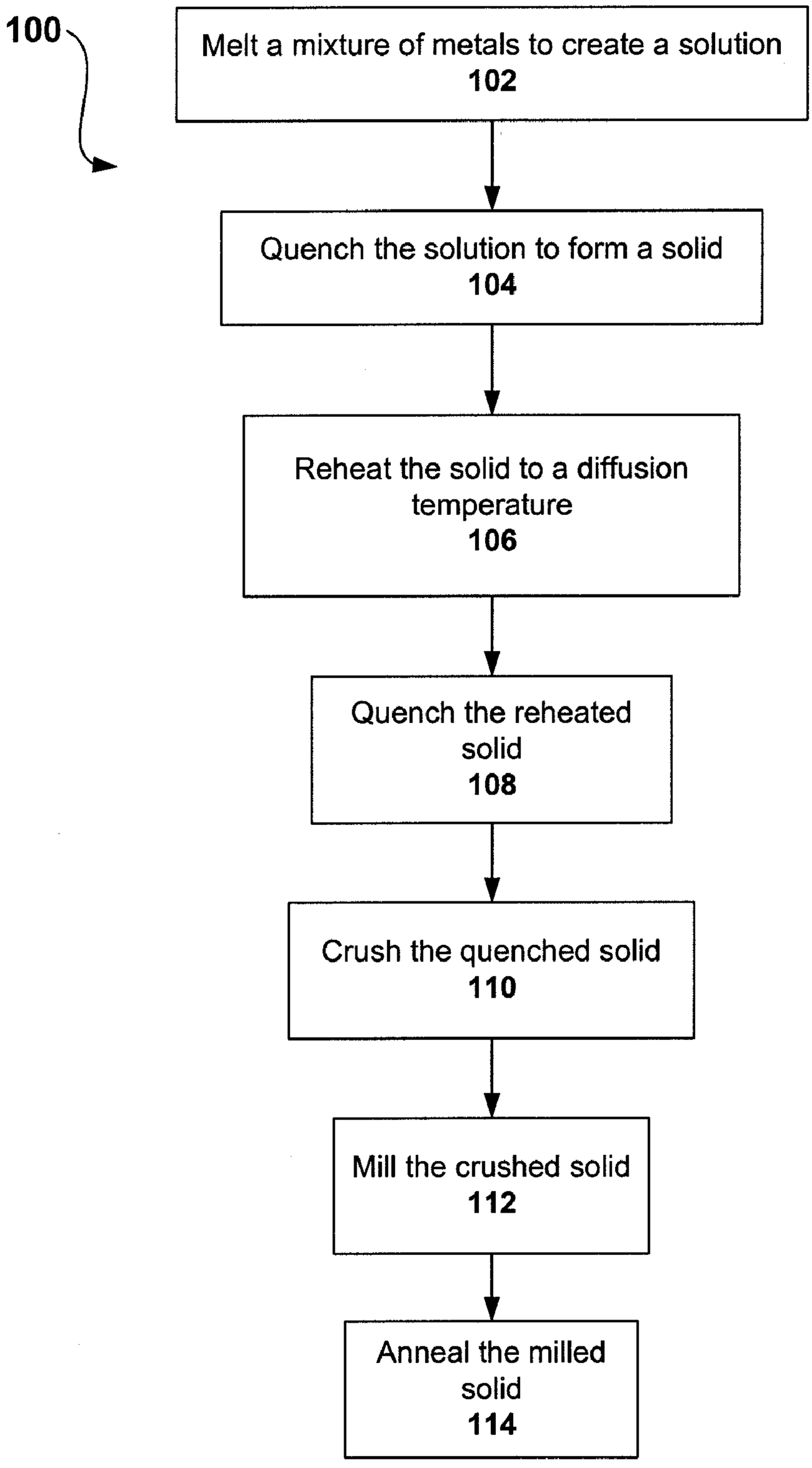
100
Melt a mixture of metals to create a solution
102
Quench the solution to form a solid
104
Reheat the solid to a diffusion temperature
106
Quench the reheated solid
108
Crush the quenched solid
110
Mill the crushed solid
112
Anneal the milled solid
114

FIG. 1

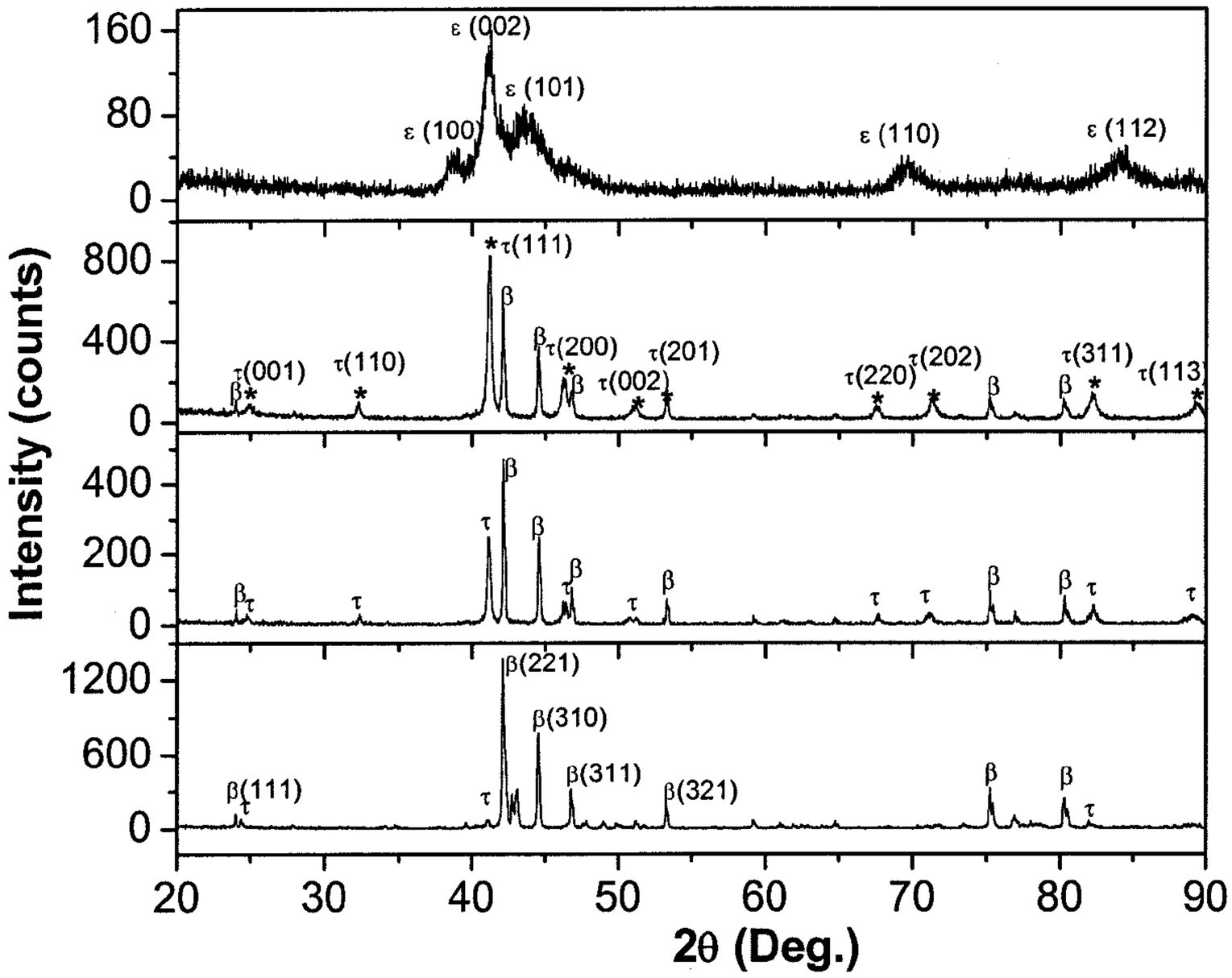

FIG. 2

FIG. 3

FIG. 4

FIG. 5

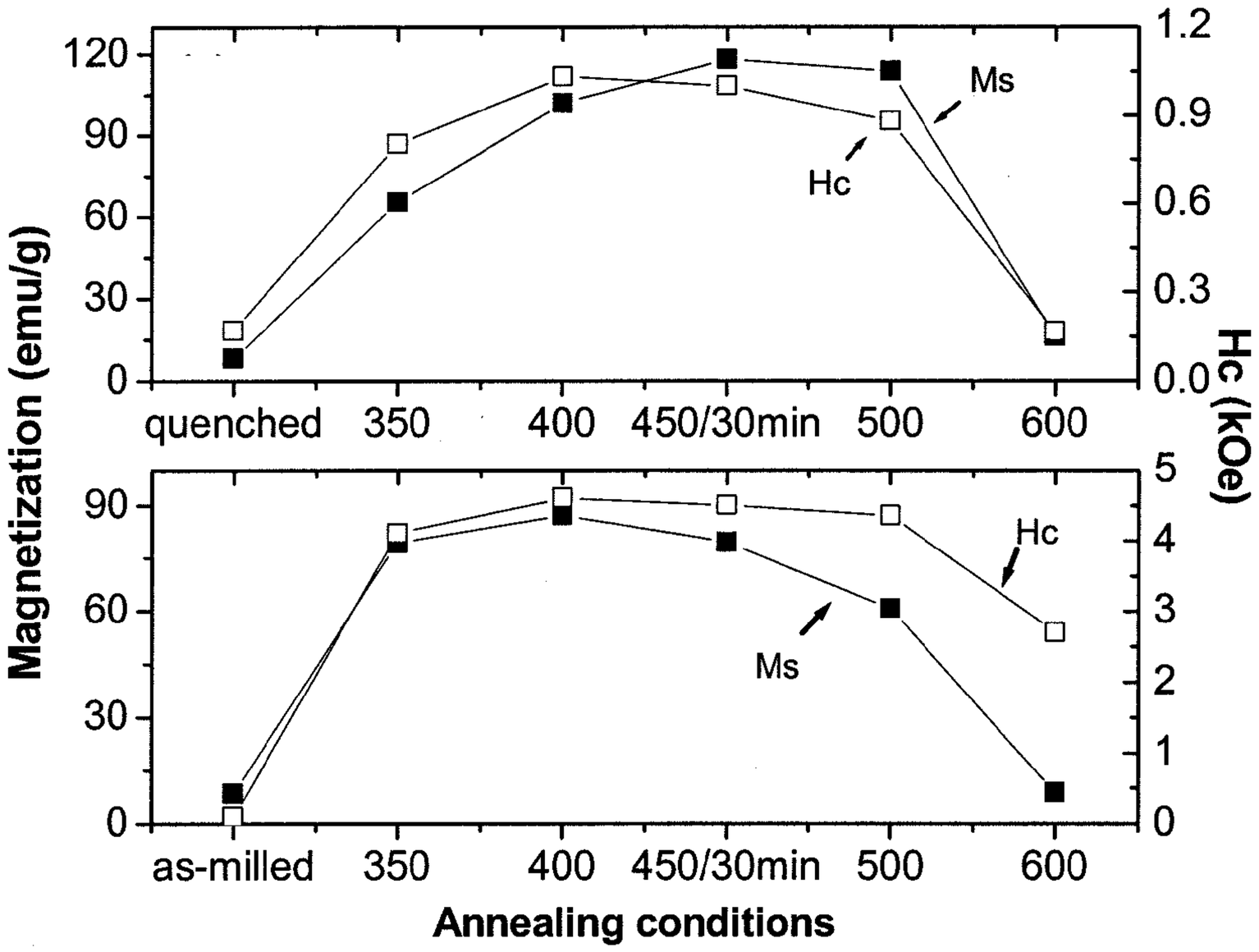

FIG. 6

FIG. 7

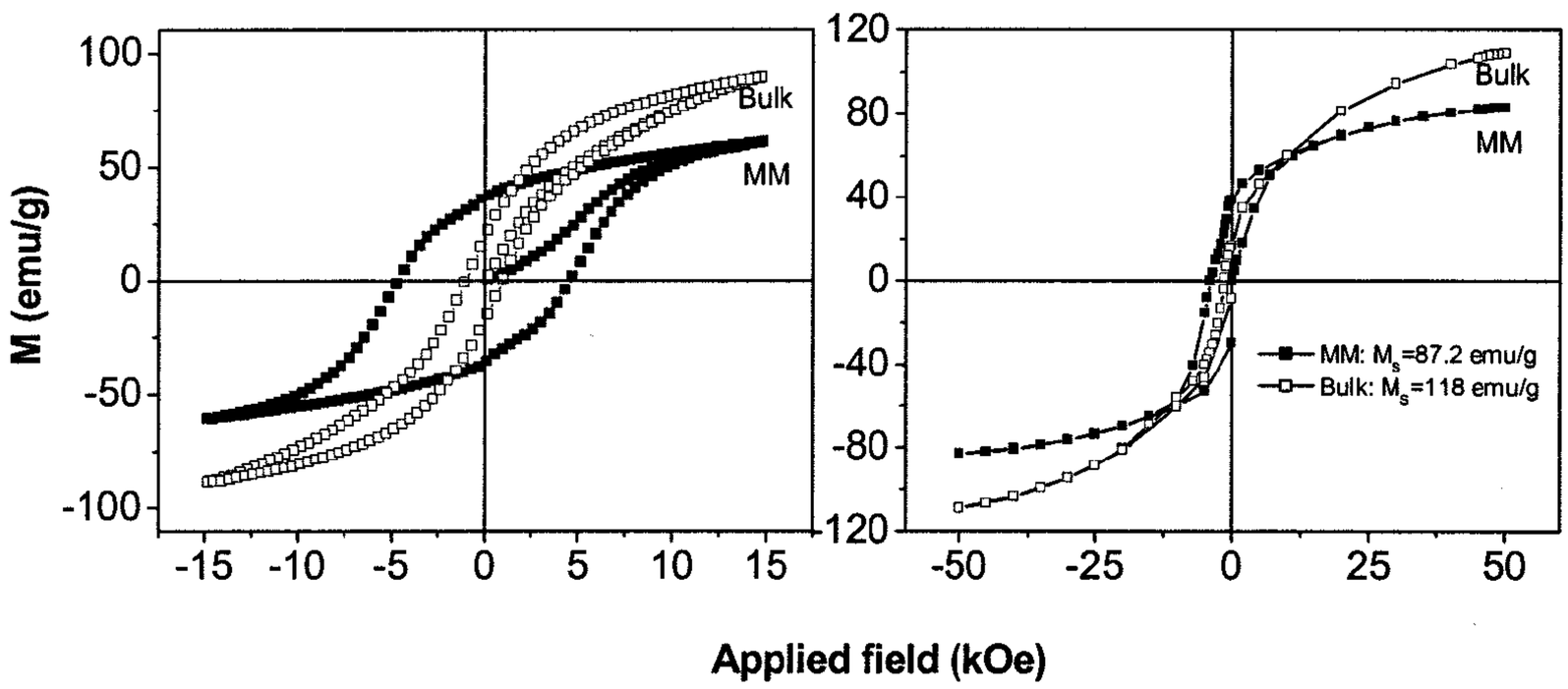

FIG. 8

FIG. 9

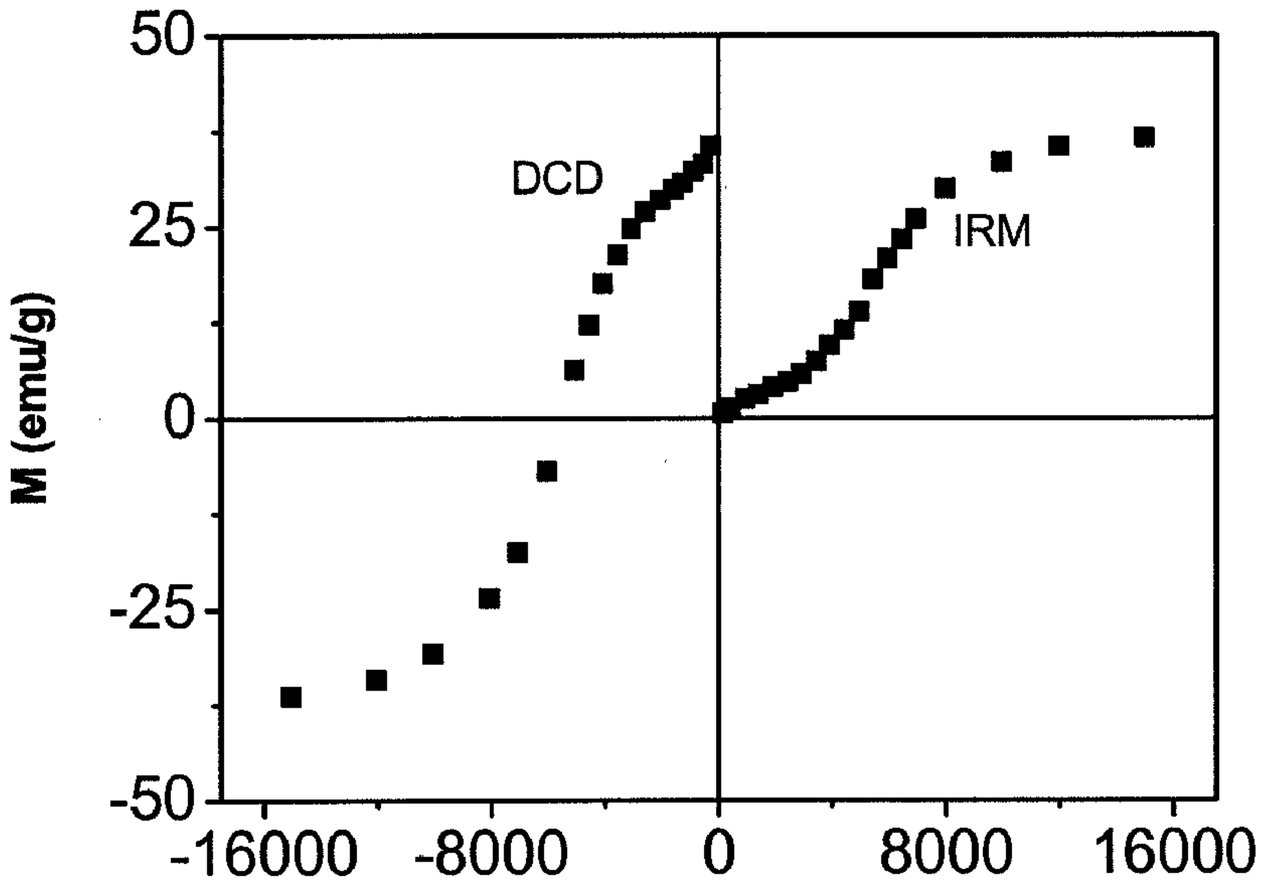
50
25
0
-25
-50
M (emu/g)
DCD
IRM
-16000
-8000
0
8000
16000

FIG. 10

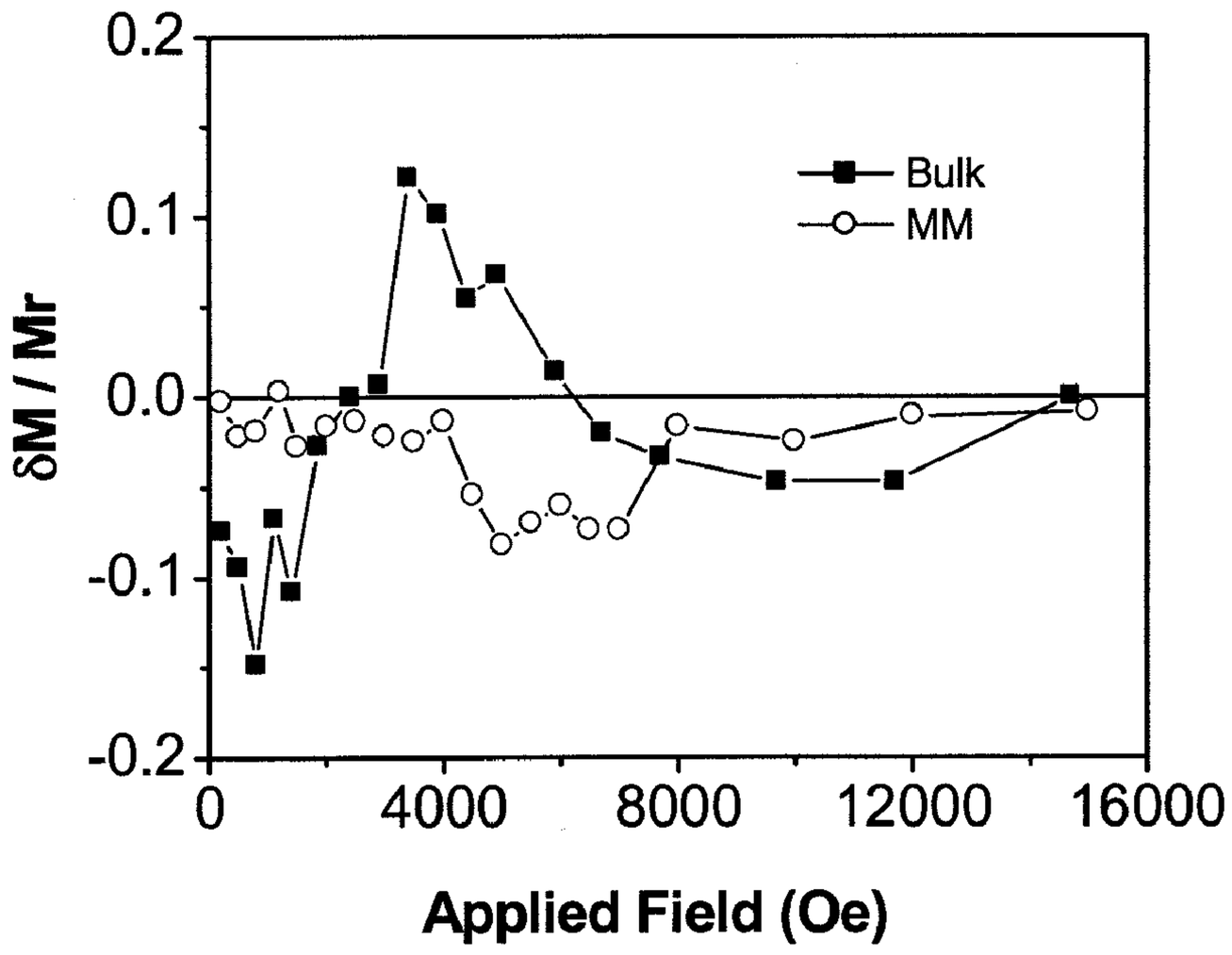
0.2
0.1
0.0
-0.1
-0.2
δM / Mr
Bulk
MM
0
4000
8000
12000
16000
Applied Field (Oe)

FIG. 11

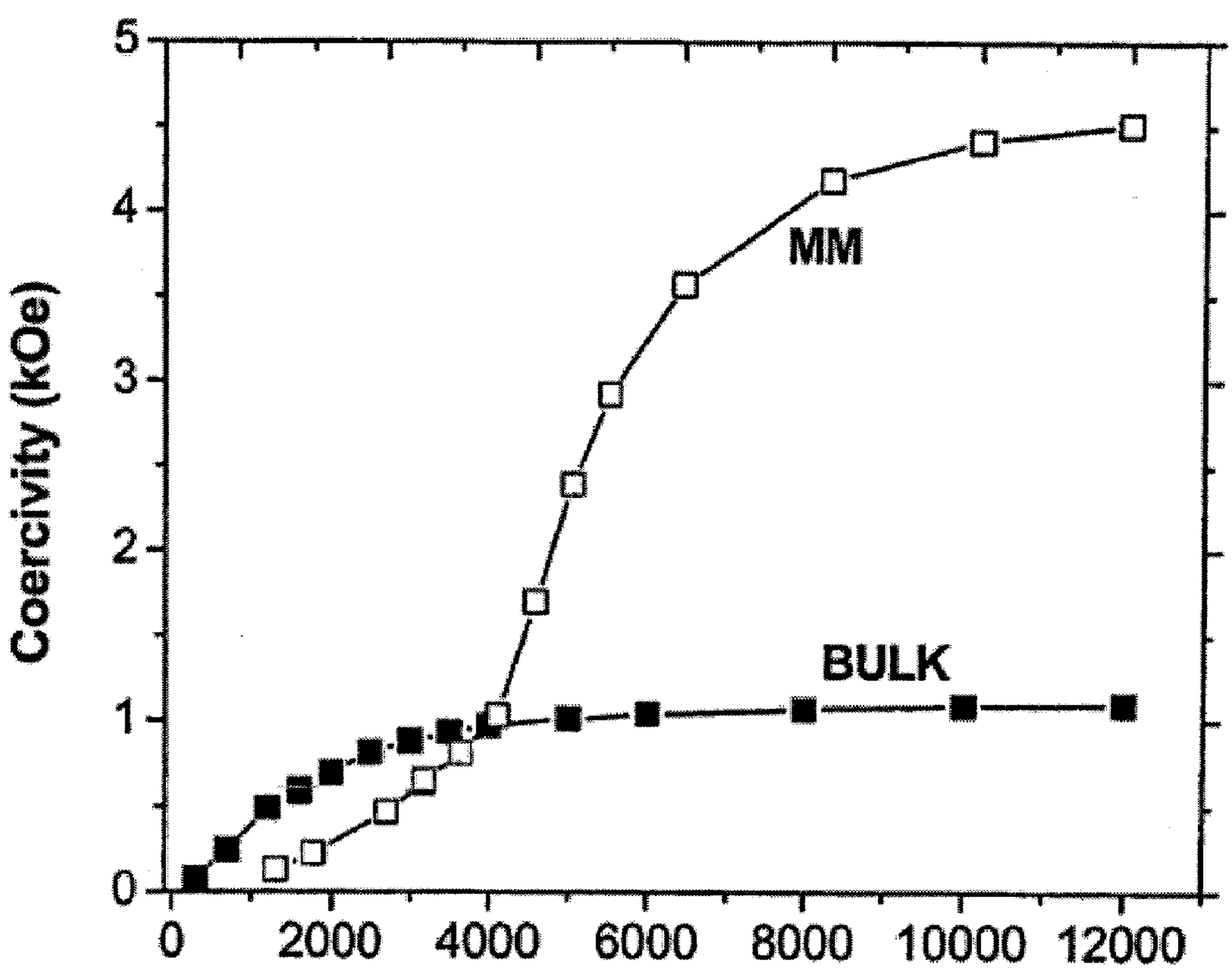
Coercivity (kOe)
0
1
2
3
4
5
MM
BULK
0
2000
4000
6000
8000
10000
12000
Applied field (Oe)

FIG. 12

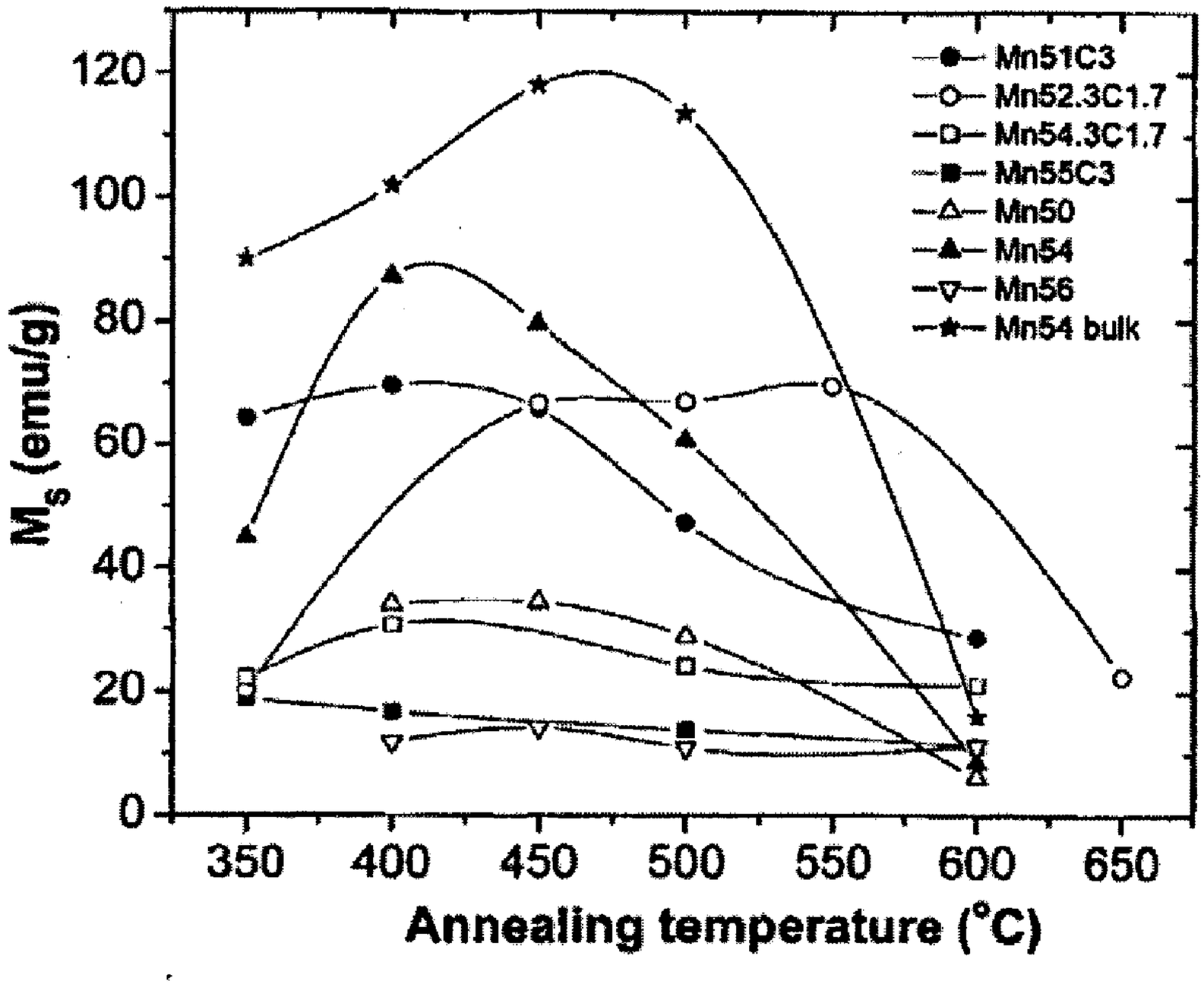
Mn51C3
Mn52.3C1.7
Mn54.3C1.7
Mn55C3
Mn50
Mn54
Mn56
Mn54 bulk
M_s (emu/g)
0
20
40
60
80
100
120
350
400
450
500
550
600
650
Annealing temperature (°C)

FIG. 13

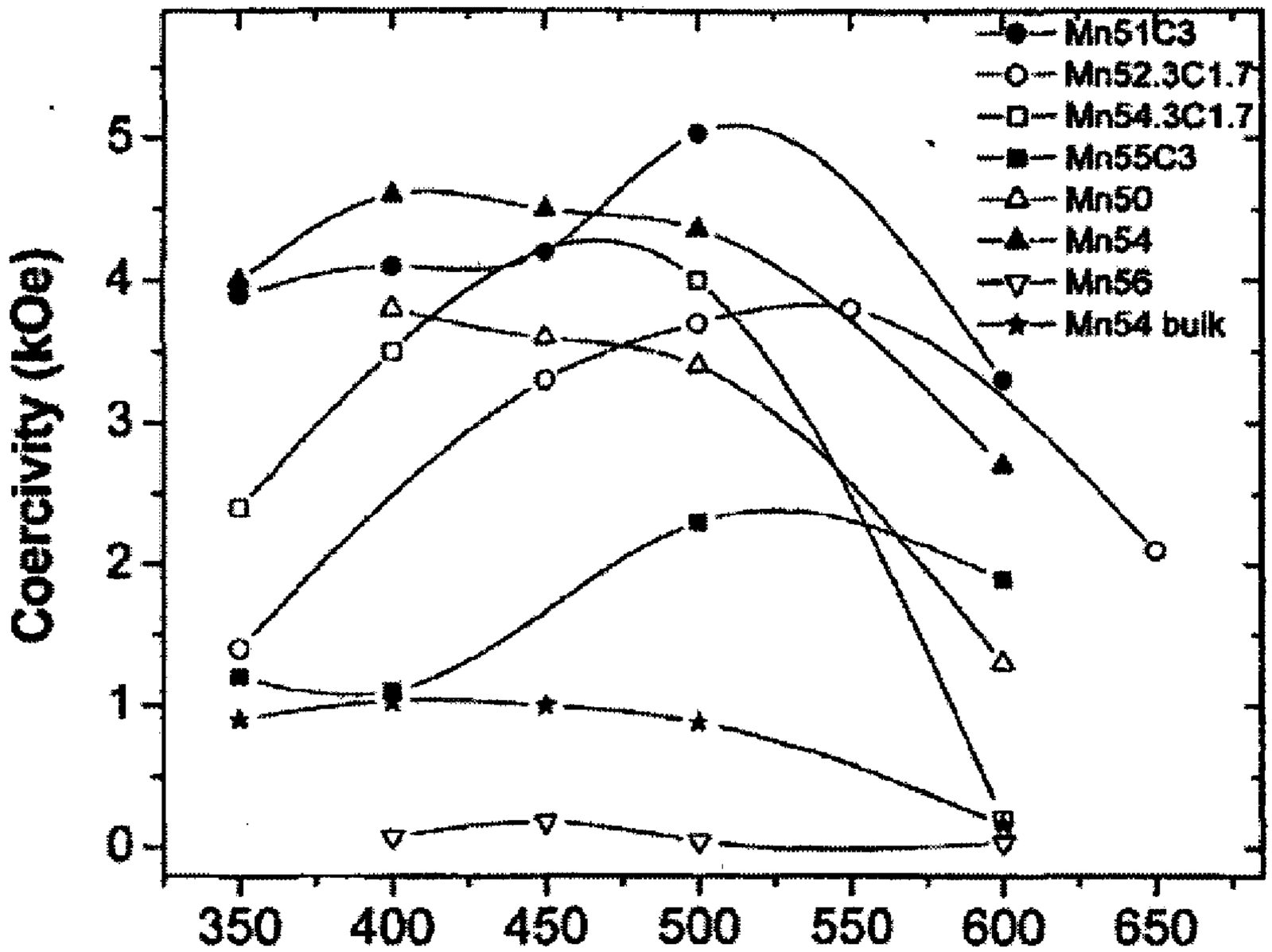
Mn51C3
Mn52.3C1.7
Mn54.3C1.7
Mn55C3
Mn50
Mn54
Mn56
Mn54 bulk
Coercivity (kOe)
0
1
2
3
4
5
350
400
450
500
550
600
650
Annealing temperature (°C)

FIG. 14

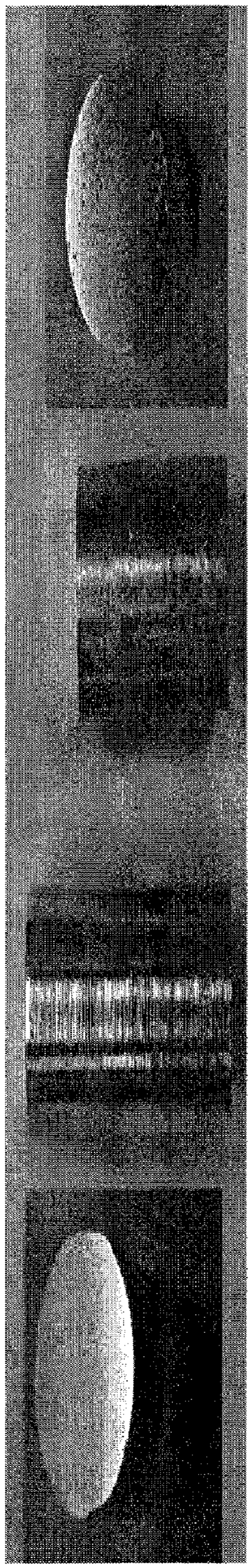

Fig. 15 (b)

Fig. 15 (a)

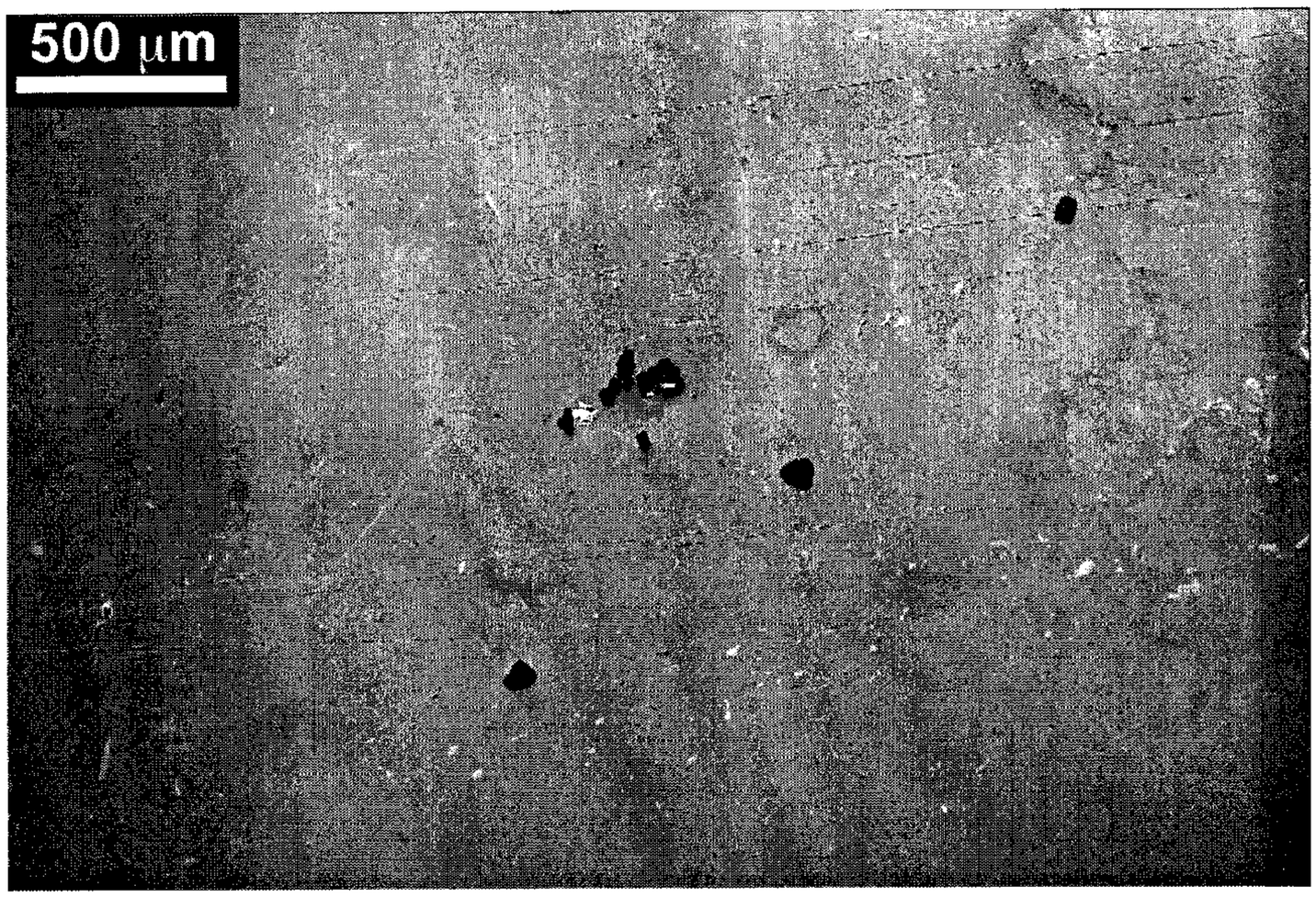

FIG. 16 (a)

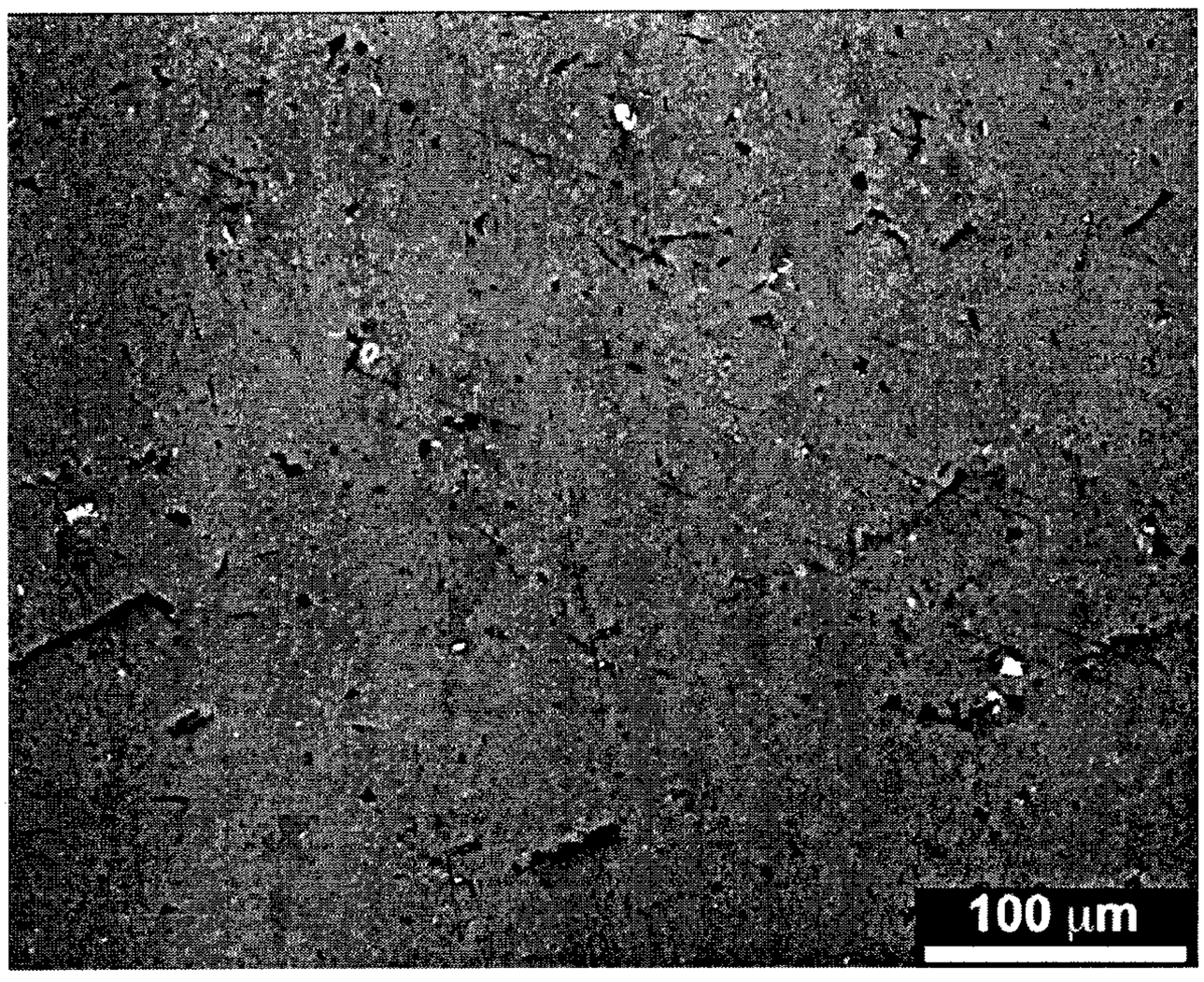

FIG. 16 (b)

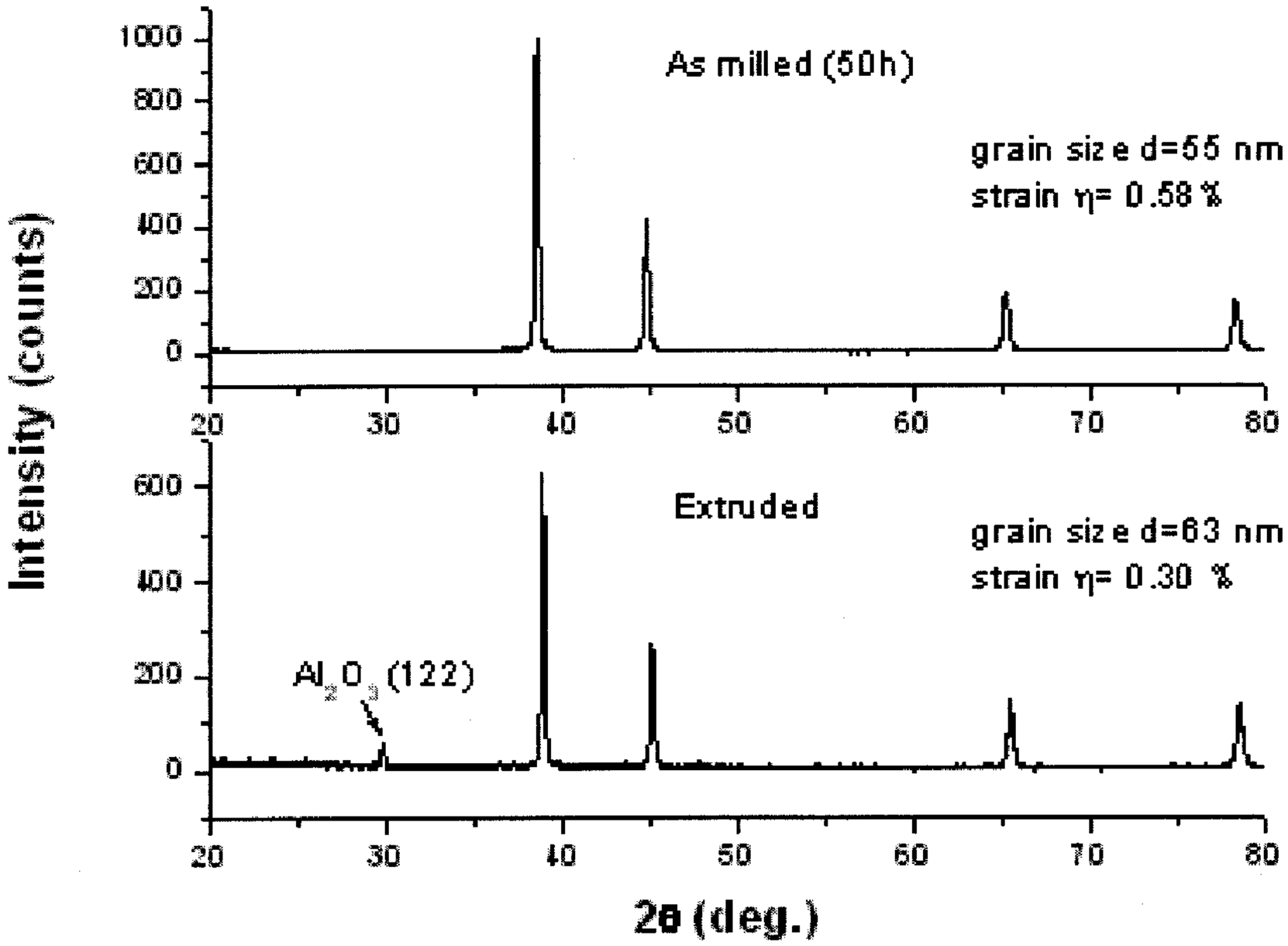
As milled (50h)
grain size d=55 nm
strain η= 0.58 %
Extruded
grain size d=63 nm
strain η= 0.30 %
Al2O3 (122)
Intensity (counts)
2θ (deg.)
0
200
400
600
800
1000
20
30
40
50
60
70
80

FIG. 17

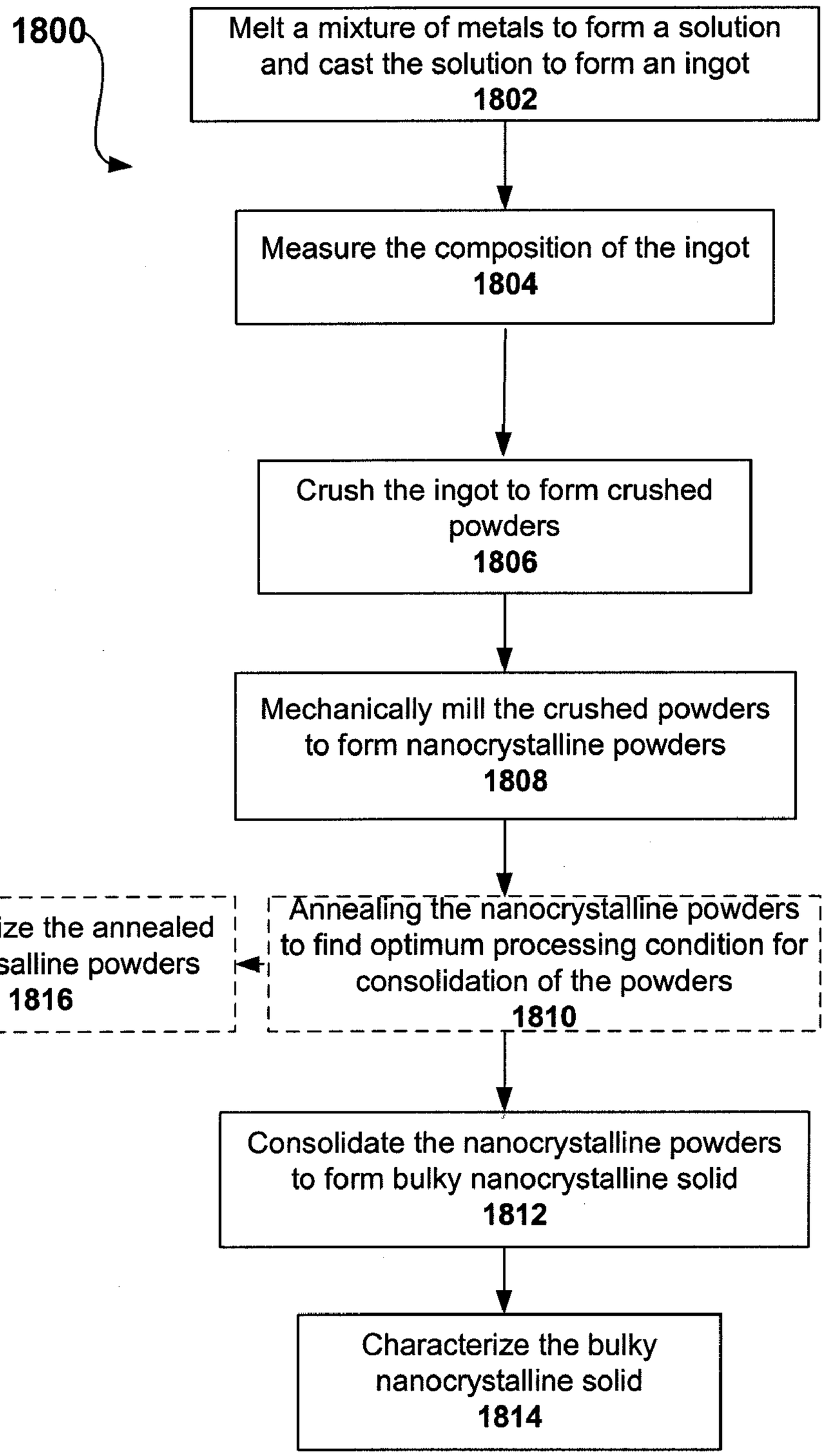
1800
Melt a mixture of metals to form a solution and cast the solution to form an ingot
1802
Measure the composition of the ingot
1804
Crush the ingot to form crushed powders
1806
Mechanically mill the crushed powders to form nanocrystalline powders
1808
Annealing the nanocrystalline powders to find optimum processing condition for consolidation of the powders
1810
Characterize the annealed nanocrytsalline powders
1816
Consolidate the nanocrystalline powders to form bulky nanocrystalline solid
1812
Characterize the bulky nanocrystalline solid
1814

FIG. 18

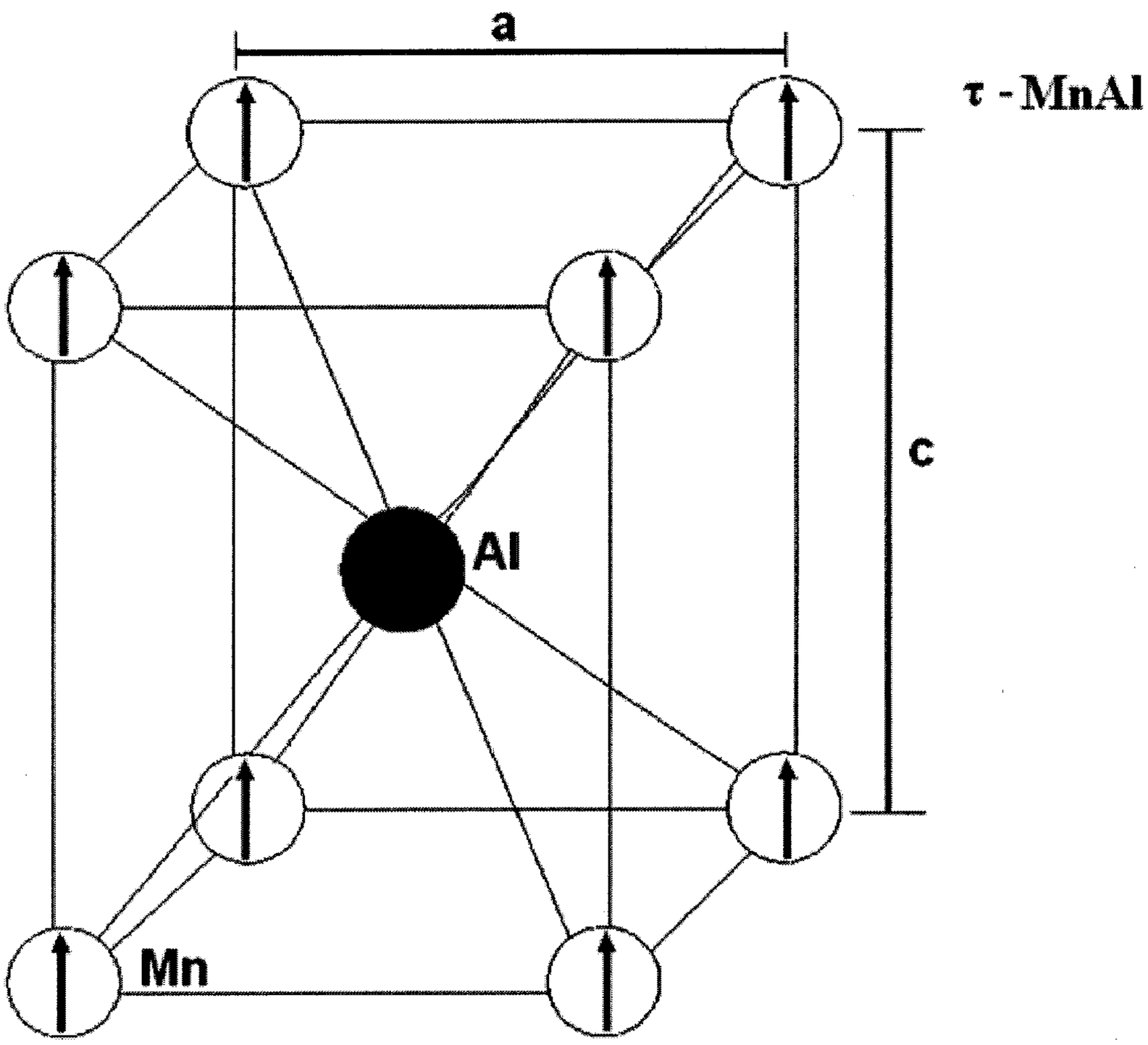

FIG. 19

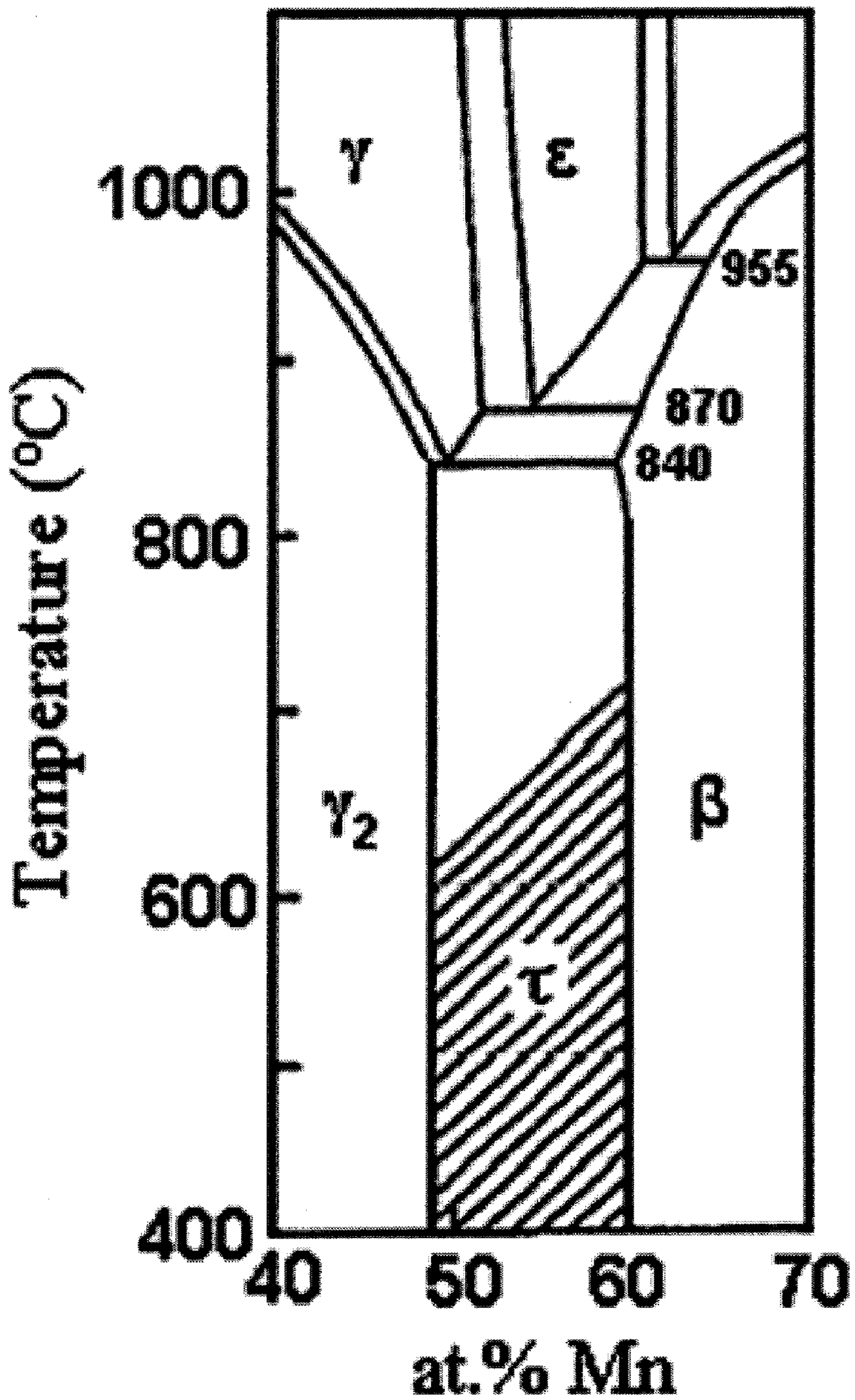
1000
800
600
400
Temperature (°C)
γ
ε
955
870
840
γ2
τ
β
40
50
60
70
at.% Mn

FIG. 20

NANOSTRUCTURED MN-AL PERMANENT MAGNETS AND METHODS OF PRODUCING SAME

RELATED APPLICATIONS

[0001] This application is a continuation in part of U.S. patent application Ser. No. 12/089,876, filed Apr. 23, 2011 which is a U.S. National Phase Application of PCT Application No. PCT/US06/417 90, filed on Oct. 27, 2006, which claims priority to U.S. Patent Application No. 60/730,697, filed Oct. 27, 2005, the disclosures of which are incorporated by reference herein.

GOVERNMENT INTERESTS

[0002] This invention was made with government support under contract number 60NANB2D0120 awarded by the National Institute of Standards and Technology (NIST). The government has certain rights in the invention.

BACKGROUND

[0003] Magnets may be broadly categorized as temporary or permanent. Temporary (soft) magnets become magnetized or demagnetized as a direct result of the presence or absence of an externally applied magnetic field. Temporary magnets are used, for example, to generate electricity and convert electrical energy into mechanical energy in motors and actuators. Permanent (hard) magnets remain magnetized when they are removed from an external field. Permanent magnets are used in a wide variety of devices including motors, magnetically levitated trains, MRI instruments, and data storage media for computerized devices.

[0004] High-performance permanent magnets, such as Sm—Co (H_C=10-20 kOe) and Nd—Fe—B (H_C=9-17.5 kOe), are generally intermetallic alloys made from rare earth elements and transition metals, such as cobalt. Demand for high-performance permanent magnets for motors is increasing rapidly for applications such as wind turbine generators and motors in electric and hybrid cars. Rare-earth magnets are generally used for such challenging applications with, for example, each Toyota Prius using 1 kg of Nd and a typical wind turbine generator using 250 Kg of Nd. These rare earth magnets have highest energy product $(BH)_{max}$ of any material, where B is magnetic flux density and H is magnetic field strength.

[0005] By way of example, $Nd_2Fe_{14}B$ has the highest $(BH)_{max}$ at 45 MGOe. However, this material is not without problems. Sintered $Nd_2Fe_{14}B$ is vulnerable to grain boundary corrosion, requiring nickel or copper/nickel plating or lacquer coating. Although polymer-bonded $Nd_2Fe_{14}B$ magnets do not suffer from this grain boundary corrosion problem, they have a significantly lower energy product due to the polymer matrix.

[0006] In another example, Sm—Co magnets have a $(BH)_{max}$ of 28-30 MGOe, which is lower than that of $Nd_2Fe_{14}B$. Although Sm—Co magnets do not suffer from corrosion and can be used at higher temperatures (up to ~350° C.), they are quite brittle, prone to chipping and can fracture from thermal shock. Further issues with these materials are that over 95% of rare earths are produced in one country and there are no US-owned manufacturers of rare earth magnets. The high cost of rare earth elements and cobalt makes the widespread use of high-performance magnets commercially impractical.

[0007] Less expensive magnets are more commonly used, but these magnets generally have lower coercivity H_C i.e., their internal magnetization is more susceptible to alteration by nearby fields. For example, ferrites, which are predominantly iron oxides, are the cheapest and most popular magnets, but they have both low H_C (1.6-3.4 kOe) and low values of M_S. Similarly, Alnico alloys, which contain large amounts of nickel, cobalt and iron and small amounts of aluminum, copper and titanium, have H_C in the range of 0.6-2 kOe, which makes exposure to significant demagnetizing fields undesirable.

[0008] The ferromagnetic τ phase in a MnAl magnet was first reported by H. Kono, On the Ferromagnetic Phase in Manganese-Aluminum Systems", Journal of the Physics Society of Japan, 13 (1958) 1444 and Koch et al. "New Material for Permanent Magnets on a Base of Mn and Al", Journal of Applied Physics, 31 (1960) 75S. This material is not used commercially in bulk form, but continues to attract attention since it has an attractive combination of magnetic properties for technological applications. MnAl magnet has a theoretical energy product, $(BH)_{max}$, of 12 MGOe together with a relatively low density of 5200 kg/m^3, and thus a high density-compensated $(BH)_{max}$. In contrast, Sm—Co magnets have a relatively high $(BH)_{max}$, but also a relatively high density of ~8300 kg/m^3. Therefore, the MnAl magnet has a comparable ratio of $(BH)_{max}$/density as compared to the Sm—Co magnet. Table 1 lists a comparison of the estimated maximum energy product, density and density-compensated maximum energy product for several classes of permanent magnets.

TABLE 1

Magnet	$(BH)_{max}$ (MGOe)	Density (kg/m^3)	$(BH)_{max}$/Density (KGOe · m^3/kg)
$Ni_2Fe_{14}B$	45	7600	5.92
Sm—Co	30	8300	3.61
Mn—Al	12	5200	2.31
AlNiCo	6	7000	0.86
Ferrites	4.5	5000	0.90

[0009] While the magnetic properties of MnAl magnets are superior to conventional hard ferrites, Alnicos, and Fe—Cr—Co alloys, MnAl is not as good as the rare-earth magnets. τ-MnAl does not suffer from the issues associated with the rare-earth magnets outlined above. Advantages of MnAl magnets include low costs and excellent availability of the Mn and Al materials, good machinability, high specific strength, high modulus of elasticity, and excellent corrosion resistance.

[0010] More recently, Mn—Al—(C) alloys have been produced by mechanical alloying processes. D. C. Crew, P. G. McCormick and R. Street, *Scripta Metall. Mater.,* 32(3), p. 315, (1995) and T. Saito, *J. Appl. Phys.,* 93(10), p. 8686, (2003) have shown that adding small amounts of carbon (e.g., about 2 atomic % or less) to certain Mn—Al alloys stabilizes the metastable τ phase and improves magnetic properties and ductility. Crew et al. (1995) produced $Mn_{70}Al_{30}$ weight % and $Mn_{70.7}Al_{28.2}C_{1.1}$ weight % alloys by consolidating ball milled powders, annealing at 1050° C. and then quenching, after which the materials were no longer nanocrystalline. The resulting alloys had grain sizes of about 300-500 nm and exhibited coercivities, H_C, of 1.4 kOe and 3.4 kOe, respectively. Saito (2003), produced mechanically alloyed $Mn_{70}Al_{30}$ weight % and $Mn_{70}Al_{29.5}C_{0.5}$ weight % alloys that

had grain sizes of about 40-60 nm and coercivities of 250 Oe and 3.3 kOe, respectively. In this study, the low coercivities reflected the limited formation of the magnetic τ phase, which was determined to be 10% in $Mn_{70}Al_{30}$ and 40% in $Mn_{70}Al_{29.5}C_{0.5}$. K. Kim, K. Sumiyama and K. Suzuki, *J. Alloys Comp.*, 217, p. 48, (1995), produced MnAl alloys that were ball milled, but never annealed. The alloys displayed no hard magnetic properties with H_C of 130 Oe.

[0011] Mechanical milling (MM) has been used to synthesize a number of rare earth permanent magnet alloys, including $Nd_2Fe_{14}B$, $Nd(Fe,Mo)_{12}N_x$ and $SmCO_5$. This processing technique may be used to produce a nanocrystalline microstructure having beneficial effects on the magnetic properties. So far, only a few studies have dealt with the magnetic behavior of MM Mn—Al. In one study by Satio, "Magnetic Properties of Mn—Al System Alloys Produced by Mechanical Alloying", Journal of Applied Physics, 93 (2003) 8686, a relatively high H_C of 3.3 kOe was obtained, but the maximum M_S was only 20 emu/g. The same author Satio studied MM MnAl—C and obtained B_r=60 emu/g and H_C=1.95 kOe, see "Magnetic Properties of Mn—Al—C Alloy Powders Produced by Mechanical Grinding", Journal of Applied Physics, 97 (2005) 1. Commercial products with magnetic properties of B_r=5.75 kG, H_C=3.0 kOe and $(BH)_{max}$=7 MGOe are made by hot extrusion of annealed gas-atomized Mn—Al—C powders by Sanyo Special Steel Co. Ltd., which has been working on MnAl—C alloys for many years. These Mn—Al alloys are made from relatively inexpensive materials, but the low coercivities remain a problem.

SUMMARY

[0012] The subject matter of the present disclosure advances the art and overcomes the problems outlined above by providing nanostructured Mn—Al alloys and a method for their manufacture. Constituents of these alloys may be mechanically milled and heat-treated to form permanent room temperature magnets with high coercivities and relatively high saturation magnetization values.

[0013] In an embodiment, a bulky consolidated nanostructured manganese aluminum alloy includes at least about 80% of a magnetic τ phase and having a macroscopic composition of $Mn_XAl_YDo_Z$, where Do is a dopant, X ranges from 52-58 atomic %, Y ranges from 42-48 atomic %, and Z ranges from 0 to 3 atomic %. In a particular embodiment, the manganese aluminum alloy includes carbon having a macroscopic composition of 51 atomic % manganese, 46 atomic % aluminum and 3 atomic % carbon and has coercive forces of about 5.2 kOe. In another particular embodiment, the manganese aluminum alloy has a macroscopic composition of 54 atomic % manganese, 46 atomic % aluminum and coercive forces of about 4.8 kOe.

[0014] In an embodiment, a method for producing a bulky nanocrystalline solid is provided. The method includes melting a mixture of metals comprising between 52-58 atomic % manganese and between 42-48 atomic % aluminum to form a substantially homogenous solution. The method also includes casting the solution to form ingots, measuring compositions of the ingots, crushing the ingots to form crushed powders, and milling the crushed powders to form nanocrystalline powders. The method also includes verifying the presence of τ phase and determining the amount of the τ phase. The method further includes simultaneously consolidating the nanocrystalline powders into a bulky nanocrystalline solid and undergoing phase transformation from ϵ phase to at least 80% τ phase, β and γ_2 phases.

[0015] In a particular embodiment, the method further includes characterizing microstructure of the bulky nanocrystalline solid and measuring magnetic properties of the bulky nanocrystalline solid. The method further includes annealing the nanocrystalline powders to determine conditions for consolidating the nanocrystalline powders. The method further includes annealing at temperatures between 200° C. and 600° C. to maximize the amount of the magnetic metastable τ phase transformed from a milled nanocrystalline unstable high-temperature ϵ phase, thereby minimizing the presence of non-magnetic equilibrium β and γ_2 phases. The annealing time is shorten for higher annealing temperature to avoid decomposition of the τ-phase into the γ_2 and β phases. The step of consolidating the milled powders includes backpressure assisted Equal channel angular extrusion (ECAE). The method further includes increasing backpressure to consolidate the nanocrystalline powders. The method further includes controlling a temperature of the nanocrystalline powders within 200° C. to 600° C. during the ECAE. The method also includes decreasing rate of extrusion with increasing temperature to shorten annealing time at higher temperature to avoid decomposition of the τ-phase into the γ_2 and β phases.

[0016] In a particular embodiment, the bulky nanocrystalline solid is in a form of rod shapes. The bulky nanocrystalline solid has a cross-section in one of square, rectangular, and circular shape. The method further includes repeating the step of consolidating the nanocrystalline powders until the bulky nanocrystalline solid having minimum defects. The bulky nanocrystalline solid is machinable. The mixture of metals includes a dopant comprising at least one of carbon and boron. The mixture of metals has 54 atomic % manganese, and 46 atomic % aluminum. The mixture of metals includes 51 atomic % manganese, 46 atomic % aluminum and 3 atomic % carbon.

[0017] The benefits of the nanostructured Mn—Al and Mn—Al—C permanent magnets include high coercivities (~4.8 kOe and 5.2 kOe, respectively) and high saturation magnetization values. The benefits of the magnets also include relatively low cost and readily available raw material supplies compared to rare earth magnets.

BRIEF DESCRIPTION OF THE DRAWINGS

[0018] FIG. **1** is a flowchart illustrating a method of producing magnetic alloys according to one embodiment.

[0019] FIG. **2** shows an X-ray diffraction pattern of $Mn_{54}Al_{46}$ prior to annealing.

[0020] FIG. **3** shows an X-ray diffraction pattern of $Mn_{54}Al_{46}$ annealed at 400° C. for thirty minutes.

[0021] FIG. **4** shows an X-ray diffraction pattern of $Mn_{54}Al_{46}$ annealed at 500° C. for thirty minutes.

[0022] FIG. **5** shows an X-ray diffraction pattern of $Mn_{54}Al_{46}$ annealed at 600° C. for thirty minutes.

[0023] FIG. **6** shows room temperature dependence of saturation magnetization and coercive field on annealing temperatures for bulk un-milled samples.

[0024] FIG. **7** shows room temperature dependence of saturation magnetization and coercive field on annealing temperatures for mechanically milled samples.

[0025] FIG. **8** shows room temperature hysteresis loops in a 15 kOe field for mechanically milled (MM) and bulk $Mn_{54}Al_{46}$ powders annealed at 400° C. for ten minutes.

[0026] FIG. **9** shows room temperature hysteresis loops in a 50 kOe field for mechanically milled (MM) and bulk $Mn_{54}Al_{46}$ powders annealed at 400° C. for ten minutes.

[0027] FIG. **10** shows room temperature isothermal remanence magnetization (IRM) and dc demagnetization (DCD) curves for mechanically milled $Mn_{54}Al_{46}$ annealed at 400° C. for ten minutes.

[0028] FIG. **11** shows room temperature isothermal remanence magnetization (IRM) difference curves for bulk and mechanically milled $Mn_{54}Al_{46}$ annealed at 400° C. for ten minutes.

[0029] FIG. **12** shows the room temperature dependence of the coercive field on the magnetic field strength for mechanically milled and bulk $Mn_{54}Al_{46}$ powders annealed at 400° C. for ten minutes.

[0030] FIG. **13** shows dependence of saturation magnetization on annealing temperatures for mechanically milled and bulk samples of various composition.

[0031] FIG. **14** shows dependence of coercivity on annealing temperatures for mechanically milled and bulk samples of various composition.

[0032] FIGS. **15**(*a*) and (*b*) illustrate billets produced by ECAE of commercial Al powder (a) four passes and (b) two passes.

[0033] FIGS. **16** (*a*) and (*b*) illustrate polished surface of (a) four pass consolidated commercial Al powder and (b) two pass mechanically-milled, nanocrystalline Al powder.

[0034] FIG. **17** illustrates X-ray diffraction patterns from as-milled and ECAE-consolidated Al powder.

[0035] FIG. **18** illustrates the steps of production and characterization of bulk fully dense nanocrystalline τ-MnAl phase.

[0036] FIG. **19** illustrates a crystal structure of τ phase of MnAl.

[0037] FIG. **20** illustrates a section phase diagram of MnAl.

DETAILED DESCRIPTION

[0038] Methods for producing mechanically milled, nanostructured Mn—Al and Mn—Al—C alloys will now be shown and described. High room temperature coercivities and saturation magnetization values have been achieved for Mn—Al alloys that are produced by the presently described methods, and it has been shown that the addition of small amounts of carbon dopant (e.g., about 3 atomic % or less) to Mn—Al alloys stabilizes the metastable τ phase and improves magnetic properties.

[0039] Mechanically milled Mn—Al alloys possessing a nanostructured ferromagnetic τ phase, with H_C=4.8 kOe and M_S=87 emu/g at room temperature, were obtained by annealing $Mn_{54}Al_{46}$ powders at 400° C. for 10 minutes. The coercivity value of this alloy is the highest ever reported for Mn—Al materials. The amount of magnetic τ phase present in the annealed product is estimated from the saturation magnetization to be about 80% on the basis that M_S of the pure τ phase is about 110 emu/g. In another embodiment, a Mn—Al—C alloy, $Mn_{51}Al_{46}C_3$, prepared by the same method displayed a coercivity that is the highest ever reported for Mn—Al—C materials, H_C=5.2 kOe.

[0040] The macroscopic formulas presented herein, e.g., $Mn_{54}Al_{46}$, pertain to the overall composition, but the materials have nanostructure or microstructure of localized phase variation (e.g., γ, β, and/or τ phases). As used herein, a "nanostructured" material is a bulk solid characterized by localized variation in composition and/or structure such that the localized variation contributes to the overall properties of the bulk material.

[0041] The large coercive forces observed are believed to result from small grains of the magnetic τ phase (~30 nm) being magnetically isolated from one another. This lack of magnetic exchange coupling may result from non-magnetic phases (e.g., β, γ) inhibiting changes in the alloy's internal magnetization when an external magnetic field is applied (i.e., the non-magnetic phase(s) act as magnetic domain wall pinning sites).

[0042] The alloys disclosed herein are resistant to corrosion and may, for example, be used in applications currently utilizing known permanent magnets. In one embodiment, small particles or powders of the alloys may be produced in a resin or plastic bonded form according to known methods. The small grain size of the alloys may provide improved ductility relative to materials with larger grains.

[0043] FIG. **1** is a flowchart illustrating a method **100** of producing magnetic alloys according to one embodiment. In a first step **102**, a mixture of metals, which may be in the form of ingots, powders, ribbons, pellets or the like, is melted to provide a liquid solution. In a second step **104**, the liquid solution is quenched to form a solid solution. Steps **102** and **104** may be repeated to ensure that adequate mixing results in the formation of a substantially homogeneous solid solution. A "substantially homogenous" solution has a uniform structure or composition throughout, such that in a randomized sampling of the solution at least 95% of the samples would have consistent compositions. In step **106**, the substantially homogenous solid solution is reheated to a diffusion temperature that is just below the melting temperature of the solid. The solid is held at the diffusion temperature for a period of time that is sufficient for the solid diffusion process to reach completion. For example, the solid may be held at the diffusion temperature for twenty hours. In step **108**, the solid is quenched, e.g., with water, to halt the diffusion process, and isolate the solid without structural rearrangement that would otherwise occur in a slow cooling process. In steps **110** and **112**, the quenched solid is crushed and milled to repeatedly fracture and cold weld the particles in order to form a nanostructured material. The milling is sufficient to cause a rupture of the crystals of the alloy as well as to allow sufficient interdiffusion between the elementary components. In step **114**, the milled solid is annealed to ensure complete formation of the nanostructured magnetic alloy.

Example 1

Production of $Mn_{54}Al_{46}$

[0044] $Mn_{54}Al_{46}$ alloy ingots were prepared by arc-melting stoichiometrically balanced quantities of Mn and Al in a water-cooled copper mold (T_m≈1250-1350° C.). The melted metallic solution was then heated until melted. Quenching was performed by allowing the alloy to rapidly cool in the copper mold to a temperature of ~30° C. in approximately 10 minutes. Ingots were flipped and melted a minimum of three times under argon to ensure mixing. Ingots were subsequently heated to and held at 1150° C. for 20 hours followed by water quenching to retain the ϵ phase. The ingots were then crushed and milled for eight hours in a hardened steel vial using a SPEX 8000 mill containing hardened steels balls with a ball-to-charge weight ratio of 10:1. The vials were sealed under argon to limit oxidation. Both the as-milled powders

and the quenched bulk samples were annealed at temperatures from 350-600° C. for 10-30 minutes to produce the ferromagnetic τ phase.

[0045] The magnetic properties were measured at a room temperature of about 20° C. using a LakeShore 7300 vibrating sample magnetometer (VSM) under an external magnetic induction field of 15 kOe. Some samples were also measured with an Oxford superconducting quantum interference device (SQUID) magnetometer under a field of 50 kOe. Accuracy of the magnetic measurements is within ±2%. Therefore, magnetic data may be reported as "about" a particular value to account for ubiquitous sources of error (e.g., magnetic fields within or near the magnetometer and errors associated with weighing samples). Microstructural characterization was performed using a Siemens D5000 diffractometer with a Cu X-ray tube and a KeVex solid state detector set to record only Cu Kα X-rays.

[0046] FIGS. **2-5** show X-ray diffraction patterns of $Mn_{54}Al_{46}$ annealed at various temperatures. X-ray diffraction patterns for as-milled alloys showed peaks corresponding to the ϵ phase of the MnAl alloy, where the ϵ phase has a crystal structure of hexagonal close packed (h.c.p). As shown in FIG. **2** the diffraction peaks were broad and of low intensity, indicative of a nanocrystalline grain structure. The grain size of the ϵ phase calculated from the (111) X-ray peak using the Scherrer formula was 8 nm. Annealing the as-milled sample of $Mn_{54}Al_{46}$ at 400° C. for 30 minutes caused the ϵ phase to transform to the τ phase which has a crystal structure of face centered tetragonal (f.c.t.). FIG. **3** shows peaks indicative of the τ phase marked by asterisks. The calculated τ phase grain size was ~27 nm, which is much smaller than that produced by conventional casting, grinding or extruding. Without being bound by theory, the smaller grain size appears to result from the τ phase forming from the nanocrystalline ϵ phase. Increasing the annealing temperature to 500° C. for 30 minutes caused decomposition of the τ phase, as shown in FIG. **4** by a decrease in intensity of the τ phase peaks. Annealing at 600° C. for 30 minutes resulted in a minimal presence of the τ phase in the final product, as shown in FIG. **5**.

[0047] These results show that the improved magnetic performance may be related to small grain sizes, where the nanostructured ϵ phase material is transformed to the ferromagnetic τ phase at anneal conditions characterized by the 400° C. anneal which produced the results of FIG. **3**. The effective temperature range for this anneal is between 300° C. and 600° C., and more preferably from 350° C. to 500° C., and most preferably from 350° C. to 450° C. The smaller grain sizes are facilitated by the milling that occurs just prior to the anneal.

[0048] FIGS. **6** and **7** show the sensitivity or dependence of saturation magnetization, M_S, and coercivity, H_C, upon annealing temperatures for both bulk (FIG. **6**) and mechanically milled (FIG. **7**) $Mn_{54}Al_{46}$. For bulk samples, the M_S tends to increase with increasing annealing temperature from 300° C. to 500° C. The M_S for mechanically milled $Mn_{54}Al_{46}$ increases from 350° C. to 400° C., then decreases with increasing annealing temperature from 400° C. to 600° C. This is consistent with the X-ray diffraction data (FIGS. **3-5**) that showed the volume fraction of the magnetic τ phase decreasing with annealing temperatures above 400° C. The H_C changes relatively little from 350° C. to 500° C. for mechanically milled samples. The optimal magnetic properties for mechanically milled samples, H_C=4.8 kOe, and M_S=87 emu/g, were obtained for $Mn_{54}Al_{46}$ powders annealed at 400° C. for 10 minutes. The coercivity value of the mechanically milled alloy is the highest reported to date for Mn—Al magnetically isotropic powders. In general, the M_S obtained for annealed, mechanically milled samples was lower than that obtained in bulk samples, while the H_C was higher, due to the small τ phase grain size.

[0049] FIGS. **8** and **9** show room temperature magnetic hysteresis loops for mechanically milled (solid squares) and bulk (open squares) $Mn_{54}Al_{46}$ powders annealed at 400° C. for 10 minutes. FIG. **8** shows hysteresis loops in a 15 kOe field. Coercivity is measured as the distance along the x-axis from the origin to the intersection of the curve with the x-axis. It can be seen that the mechanically milled sample has a much larger coercivity (~5 kOe) than the bulk sample (~1 kOe). Remanent magnetization, M_r, is the intrinsic field of the sample when the applied field is zero. M_r of the mechanically milled sample is approximately 35 emu/g, while that of the bulk sample is approximately 25 emu/g. FIG. **9** shows hysteresis loops in a 50 kOe applied field. Magnetic saturization, M_S, has not been reached, as evident from the increasing magnetization at high fields. For the mechanically milled sample, the remanence ratio, M_r/M_S, is about 0.5 when the applied field is 50 kOe, which is characteristic of materials that are not exchange-coupled.

[0050] FIGS. **10** and **11** show isothermal remanence magnetization (IRM), dc demagnetization (DCD) and difference curves for mechanically milled $Mn_{54}Al_{46}$ annealed at 400° C. for 10 minutes. FIG. **10** shows the IRM and DCD curve for the mechanically milled sample, and FIG. **11** shows the δM curves for both mechanically milled and bulk samples annealed at 400° C. for 10 minutes. Remanence curves and δM plots were used to determine the interaction between the τ-phase grains. The DCD curve shows the progress of the irreversible changes in magnetization. The IRM curve contains contributions from both reversible and irreversible magnetization processes. The change of magnetization δM is defined as:

$$\delta M = M_d(H) - [M_r(H_{sat}) - 2M_r(H)] \quad \text{Equation (1)}$$

where M_d (H) is the demagnetic remanent magnetization, M_r is remanent magnetization, and H_{sat} is magnetic field strength that saturates the magnet.

[0051] A plot of δM versus H therefore gives a curve characteristic of the interactions present. The overall negative and small δM for the mechanically milled sample indicates that most of the τ phase nanograins are isolated with only small dipolar interactions between them. No exchange coupling exists in this nanostructured material, which explains why the remanence ratio is close to 0.5.

[0052] FIG. **12** shows the dependence of the coercive field on the magnetic field strength for mechanically milled and bulk $Mn_{54}Al_{46}$ powders annealed at 400° C. for 10 minutes. The bulk sample curve rises steadily to near saturation. In contrast, the mechanically milled sample curve rises gradually at low fields until the field strength approaches H_C (5 kOe), then it rises quickly to near saturation. This behavior indicates that the mechanism for the magnetization process of the mechanically milled material is controlled by domain wall pinning, and that the applied field gradually removes the domain walls from their pinning sites. The non-magnetic phase(s) that are present could act as the pinning sites.

Example 2

Alloy Content Sensitivity

[0053] The manufacturing process of Example 1 was repeated by varying the content of the Mn and Al metals, and

doping with carbon. FIGS. **13** and **14** show the dependence of saturation magnetization and coercivity on annealing temperatures for mechanically milled and bulk samples of various composition after the samples had been annealed for thirty minutes. The legends of FIGS. **13** and **14** show Mn content, and optionally C content, where the remainder of the sample is Al. All samples are mechanically milled, except for those labeled "bulk". It can be seen that 1-3 atomic % carbon decreased M_S but increased H_C in some cases. In particular, $Mn_{51}Al_{46}C_3$ had the highest H_C observed to date for a Mn—Al—C alloy, 5.2 kOe. Dopants other than carbon may include boron. Generally, it can be noted that because the τ phase is the only ferromagnetic phase in the Mn—Al or Mn—Al—C systems, the saturation magnetization is proportional to the percentage of the ϵ phase in the alloys. When the Mn content is 50 atomic percent or less, little ϵ phase can be developed, and therefore only a small amount of τ phase can be produced. Also, when the Mn content is high, excess Mn is used to stabilize the metastable τ phase. In this case, some Mn atoms occupy lattice sites where they are coupled antiferromagnetically to other nearby Mn atoms, thereby reducing the magnetization. Thus, the Mn content is preferably between 52 and 58 atomic percent and the alloys may be described according to Formula (I):

$$Mn_XAl_YDo_Z, \quad (I)$$

[0054] where Do is a dopant that may include carbon, boron, X ranges from 52-58 atomic %, Y ranges from 42-48 atomic %, and Z ranges from 0 to 3 atomic %. In preferred embodiments, Do is carbon, X ranges from 53-56 atomic %, Y ranges from 44-47 atomic %, and Z ranges up to 3 atomic %. In a most preferred embodiment, X is 54, Y is 46, and Do is not necessarily present.

Example 3

Powder Consolidation by ECAE

[0055] The disclosure presents methods for producing nanocrystalline τ-phase MnAl with a coercivity, H_c, of 4.8 kOe, and a saturation magnetization, M_S, of 87 emu/g by mechanically-milling powders of the unstable, high-temperature ϵ-phase until they were nanocrystalline and then annealing the milled powders. These values are the highest reported for Mn—Al based powders (bulk magnets have M_S of 110 emu/g). Good magnetic properties resulted from producing the nanocrystalline ϵ-phase first and then transforming the ϵ-phase into the τ-phase rather than producing the τ-phase and then milling τ-phase to produce nanocrystalline material as conventionally undertaken. The origin of the high H_c may be the nanostructure and/or the presence of small amounts of the equilibrium γ_2 and β phases, which could pin the magnetic domain walls.

[0056] While this improvement in magnetic properties is exciting, the powders should be consolidated while retaining their good magnetic properties in order for the material to be of practical value. The heat treatment to which the milled ϵ-phase powders have to subject in order to produce the superior magnetic behavior provides a processing window to allow the warm consolidation of the powders. This disclosure presents methods for consolidating nanocrystalline MnAl powders into a fully dense solid while producing the superior magnetic properties that can be obtained in the powders.

[0057] The present disclosure further includes methods of producing anisotropic magnets by warm extrusion, determination of the origin of the high H_c so that the heat treatment and composition of the powders can be optimized to develop even better magnetic properties. The milled nanocrystalline ϵ-phase powders, with this heating, simultaneously consolidate to form a bulky solid and undergo the necessary phase transformations to form the required microstructure.

[0058] Equal channel angular extrusion (ECAE) is a powder consolidation technique to consolidate microcrystalline powders by Kim et al, "Equal Channel Pressing of Metallic Powders", Materials Science Forum, 437-438 (2003) 89 and Xiang et al, "Microstructure and mechanical properties of PM 2024Al-3Fe-5Ni alloy consolidated by a new process, equal channel angular pressing", Journal of Materials Science Letters, 16 (1997) 1725. Further, the use of backpressure has been reported to be effective in aiding the compaction of Mg alloy powders and shavings to full density by Lapovok, "The positive role of back-pressure in equal channel angular extrusion", Materials Science Forum, 503-504 (2006) 37.

[0059] ECAE was used to consolidate commercial Al powders, eutectic Al—Si powders, unalloyed Mg powders and nanocrystalline Al powders. The powders were cold-compacted into annealed copper cans, onto which lids were pressed. Then, the cans were extruded at about 200° C. through a well-lubricated hardened-steel ECAE jig. A key to successful consolidation was to have a brass plug in front of the copper can to provide backpressure during extrusion. Extrusion without the plug led to poor powder consolidation, particularly for the milled Al.

[0060] FIGS. **15**(*a*) and **15**(*b*) show billets that are 12.5 mm diameter cylinders produced from Al powder extrusion through the ECAE jig after (a) four ECAE passes and (b) two ECAE passes. FIGS. **16**(*a*) and **16**(*b*) show polished surfaces after (a) four ECAE passes and (b) two ECAE passes. Note that FIG. **16** (*a*) shows a smoother polished surface than FIG. **16**(*b*). By increasing the number of passes, fewer pores were observed in FIG. **16**(*a*) than in FIG. **16** (*b*). After four passes the Al was almost at full theoretical density, and the Al was close to its full theoretical density even after two passes.

[0061] An important feature of the consolidation of the mechanically-milled Al powder is that the nanocrystalline grain size of 55 nm produced by mechanical milling only marginally increased during the ECAE extrusion to a grain size of 63 nm (see FIG. **17**) demonstrating the usefulness of this approach for producing bulk nanocrystalline materials.

[0062] ECAE was also used to consolidate Mg-alloys without using a can, i.e. the powder is loaded directly into the jig, reported by Baker et al, "Containerless Consolidation of Mg Powders using ECAE", Materials and Manufacturing Processes, 25(12) (2010) 1381-1384, which is incorporated by reference herein. Commercial Mg can be consolidated to full density after two passes through the ECAE jig at 200° C.

[0063] ECAE can also be used to consolidate MnAl powders to form a bulky MnAl solid in a way similar to consolidation of Mg powders or Al powders. Extrusion may be performed at relatively lower temperatures than is the case with conventional hot extrusion, in order to avoid allowing the ϵ phase to fully transform to the equilibrium β and γ_2 phases during consolidation. The temperature is a compromise between being as low as possible to prevent significant grain growth and high enough to allow powder consolidation. Variation in ECAE for consolidating MnAl powders may include temperatures at which extrusion occur, the powders are consolidated with and without a can, with a plug to provide backpressure etc.

[0064] It should be noted that the nanocrystalline powders are simultaneously consolidated and undergo the necessary phase transformations from ϵ phase to magnetic τ phase and non-magnetic β and γ_2 phases to form the required microstructure. The magnetic τ phase is at least 80%. The coercivity Hc of the bulky nanocrystalline solid remains substantially unchanged from the nanocrystalline powders. Specifically, MnAl bulky nanocrystalline solid can have a Hc of 5.2 kOe for 51 atomic % manganese, 46 atomic % aluminum and 3 atomic % carbon, and a Hc of 4.8 kOe for 54 atomic % manganese, 46 atomic % aluminum.

Example 4

Production of Bulk Fully Dense Nanocrystalline MnAl Solid

[0065] The relevant MnAl phase transformations simultaneously consolidate nanocrystalline ϵ-MnAl phase powders and transform them to the magnetic τ-MnAl phase. Understanding the origin of the high H_c in nanocrystalline τ-MnAl phase assists processing and composition of the powders to optimize magnetic properties. A working hypothesis is that it is the nanoscale distribution of the non-magnetic β and γ_2 phases that produces the high H_c, via domain-wall pinning, in nanostructured τ-MnAl magnets.

[0066] FIG. **18** illustrates steps of production and characterization of bulk fully dense nanocrystalline τ-MnAl phase. The steps include the production of nanocrystalline MnAl powders, their subsequent heat treatment; their consolidation using backpressure-ECAE. The bulky solids are then characterized for their magnetic properties using a vibrating sample magnetometer (VSM), and for their microstructure using scanning electron microscopy (SEM) coupled with electron backscattered patterns, transmission electron microscopy (TEM) coupled with energy dispersive X-ray spectroscopy (EDS) and convergent beam electron diffraction (CBED), and atom probe tomography (APT).

[0067] At step **1802**, casted ingots are produced from as-received mixtures in the form of powders, flakes, pellets, ribbons or the like (~100 g) of several compositions of Mn—Al near the $Mn_{54}Al_{46}$ composition with or without carbon. The as-received mixtures are arc melted and cast into a chilled copper mold to form an ingot. Melting and casting each ingot three times and flipping the ingot over in between may improve the homogeneity. Since Mn has a low vapor pressure and can easily be lost during melting, the compositions of the alloys is measured at step **1804**, including the oxygen and carbon content, after melting using a wet chemistry approach. Typically, excess Mn is added to the starting materials to compensate for any losses of Mn. The ingot contains ϵ-MnAl.

[0068] At step **1806**, the ingot is crushed into powders to prepare for mechanical mill. The crushed powders have relatively large grain sizes in the range of microns. Mechanical mill reduces the grain sizes of the crushed powders to nanometer ranges, while the ϵ-phase of the MnAl alloy remains unchanged during crushing and mechanical milling

[0069] At step **1808**, nanocrystalline powders are produced by mechanically milling the crushed powders using a water-cooled Union Process Szegvari attritor. Typically a rotation speed of approximately 700 rpm is used with hardened steel balls for 30-40 hrs under an argon atmosphere. 50-100 g of powders are milled, with a ball-to-powder ratio of 10:1. A SPEX mill may be used to more rapidly (~8 h) produce nanocrystalline material than the attritor, but only around 5 g of material are produced and more contamination of the powder tends to occur with the SPEX. The milled powders are now nanocrystalline ϵ-MnAl powders.

[0070] An understanding of the kinetics of the transformation may inform about the conditions to use for the consolidation of the nanocrystalline powders. It is much easier to run many different anneals on the powders and to determine the phases present and the magnetic properties than to have many consolidation runs and determine microstructure and magnetic properties.

[0071] Nanocrystalline ϵ-MnAl powders may be optionally annealed at different temperatures and times to determine the optimum processing conditions for the best magnetic properties at step **1810**. The step **1810** is bounded in dash lines to indicate that this is an optional step. The starting point for the heat treatments is a 30 min anneal at 400° C. in a particular embodiment. However, powders may be annealed for very short time at higher temperature and for longer time at lower temperature. Powders may also go through two-step anneals of different times at different temperatures. Annealing temperature may be from 200° C. to 600° C. These anneals intend to maximize the amount of the magnetic metastable τ phase transformed from the as-milled, nanocrystalline unstable high-temperature ϵ phase, thereby minimizing the amounts of the non-magnetic equilibrium β and γ_2 phases present. If it is the nanoscale distribution of the non-magnetic β and γ_2 phases that produces the high H_c in MnAl, via domain-wall pinning, a small amount of finely distributed β and γ_2 has also to be present.

[0072] At step **1812**, the nanocrystalline ϵ-MnAl powders are consolidated into a bulky nanocrytsalline solid, which includes at least 80^% of τ phase and presence of β and γ_2 phases. The solid may be in a shape of rod. The rod may have a cross-section in any shape including square, rectangular, circular, etc. It will be appreciated by those skilled in the art that the shape and dimension may vary for the nanocrystalline solid.

[0073] For consolidation of nanocrystalline powders, the ECAE system includes the ECAE jig, cartridge heaters with thermocouple feedback to control the temperature, and forward and backpressure pistons. A variety of temperatures are used, based on the powder annealing results outline above, in order to consolidate the powder. Higher backpressure is generally better for powder consolidation. The powders may be consolidated in one pass or two or more passes if a previous pass is unsuccessful. The consolidated bulky nanocrystalline solid should have minimum defects or substantially free of defects.

[0074] It is noted that the ECAE jig produced billets that are about 15 mm diameter and 40 mm long. In principle, ECAE processing can simply be scaled up using a larger jig and a larger extrusion piston system, similar to a traditional direct extrusion set up. In reality, the scale up probably requires lower pressures that simply scaling with the size of the billet. The reason for this is that in small specimens the surface frictional forces in the billet have a larger effect in small diameter specimens than large diameter specimens due to the larger surface-to-volume ratio.

[0075] At step **1816**, the annealed powders may be optionally characterized for their microstructure and magnetic properties. The step **1816** is bounded in dash lines to indicate that this is an optional step. The size and morphology of the unmilled, milled and annealed powders are determined using

secondary electron imaging in a field emission gun (FEG) XL30™ scanning electron microscope by FEI company. The phases present in each of these annealed powders are determined using a computer-controlled Riagku DMax rotating anode X-ray diffractometer with a Cu target. The average grain size (and lattice strain) are calculated from the corrected full width at half maximum of each diffracted peak, β_{sample}, for the powders using a Hall-Williamson method:

$$\beta_{sample}\cos\theta = \frac{k\lambda}{\delta} + 2\varepsilon\sin\theta \qquad \text{Equation (2)}$$

Where k is Scherrer constant, δ is the grain size, λ is the wavelength, c is the internal strain introduce by milling, and θ is the Bragg angle. β_{sample} is obtained from $\beta_{sample}^2=\beta_{measured}^2-\beta_{instrument}^2$, where $\beta_{instrument}$ and $\beta_{measured}$ are the Full Width Half Maximums (FWHM) of a well-annealed and a milled specimen, respectively.

[0076] At step **1814**, the bulky MnAl solid is characterized for its microstructure and magnetic properties. For microstructural characterization of extruded bulky MnAl solid, a FEI Tecnai F2 FEG 200 keV transmission electron microscope (TEM) is used. Energy dispersive X-ray microanalysis (EDS) and convergent beam electron diffraction (CBED) are performed using this instrument. Several microstructural features are analyzed to determine the crystal structures of the phases present using CBED, including whether any ϵ-MnAl is left over after the processing. The chemistry of the phases are measured using EDS. The grain size of the τ-MnAl phase is determined using bright field imaging. The sizes of the β and γ_2 particles are determined using dark field imaging. The distribution of the β and γ_2 particles, i.e. whether they are homogeneously distributed, lie on the τ-MnAl grain boundaries or lie in lines along the extrusion direction, are determined using dark field imaging. The orientation relationships between the τ-MnAl matrix and the β and γ_2 particles are determined. The coherency of the β and γ_2 particles with the τ-MnAl matrix are determined. The dislocation density in the τ-MnAl matrix are determined using a standard point line-intersection counting method coupled with measurements of the foil thickness using the standard two-beam CBED technique. The Burgers vectors of the dislocations are determined using tilting experiments and the standard g.b=0 (where g is the diffraction vector and b is the dislocation Burgers vector) invisibility criterion.

[0077] When the phases present are small, such as within a few nanometers, EDS may not be very useful for determining their chemistry. In this case, a Cameca Local electrode atom probe (LEAP) located at Oak Ridge National Laboratory (ORNL) is used. In the LEAP, a high electric field is applied to a sharp needle-shaped specimen, held in a high vacuum, to strip individual atoms from the specimen atom layer by atom layer over thousands of layers and identify them—including their location—by time-of-flight mass spectrometry. The LEAP is somewhat complementary to the TEM since it does not provide diffraction data.

[0078] Fine precipitates can be identified by using atom probe tomography (APT). The compositions of fine particles can be determined using the APT. The extruded MnAl alloy may have a texture. Thus, the grain orientations and grain misorientations are determined using electron backscatter patterns (EBSPs) using the FEI FEG XL30 SEM.

[0079] For magnetic measurements, the quasi-static magnetic behavior of the powders and consolidated MnAl may be measured using a Lakeshore Instruments 7300 VSM that can apply fields up to 15 kOe. This field strength cannot saturate the alloys, thus the M_S will be determined by extrapolation of $H^{-2}\rightarrow 0$, from a plot of the saturation law $M=M_S(1-a/H^2)$. The warm extrusion via ECAE may produce anisotropic magnets which have improved magnetic properties compared to isotropic magnets.

[0080] To interpret the measurements, a key question is whether the τ-phase has to be nanocrystalline to get the superior magnetic properties as seen in annealed powders, or whether it is sufficient to have the equilibrium β and γ_2 phases distributed on the nanoscale if these β and γ_2 phases are the cause of domain wall pinning and, hence, the high H_c. Extruding the nanocrystalline powders at different temperatures may lead to a wide variety of microstructures, i.e. different τ grain structures and different distributions of the non-magnetic equilibrium β and γ_2 phases. From analyzing these microstructures and correlating them with the measured magnetic properties, processing of the material can be improved and better compositions can be determined.

[0081] FIG. **19** illustrates a crystal structure of τ phase of MnAl. The crystal structure is tetragonal. The c/a ratio is close to 1. The arrows indicate the magnetic dipoles. FIG. **20** illustrates a section phase diagram of MnAl. Note that MnAl has a high-temperature ϵ-phase, low-temperature equilibrium γ_2 and β phases, and a metastable τ phase.

[0082] It is known that Mn metal is ordinarily antiferromagnetic. By increasing the atomic distance between Mn atoms to 2.96 Å or more, the element becomes ferromagnetic. The ferromagnetism of the τ-phase in MnAl occurs because the magnetic moments of Mn atoms in 0, 0, 0 sites are parallel to one another (see FIG. **19**).

[0083] Although various mechanisms have been proposed for τ-phase formation, the generally accepted one is that the high-temperature non-magnetic ϵ-phase (h.c.p.) transforms into a non-magnetic ϵ'-phase (orthorhombic) by an ordering reaction, and then transforms into a ferromagnetic τ-phase by a martensitic phase transition, i.e. ϵ→ϵ**40** ∝τ. However, the transformation from ϵ to τ may also involve diffusion, and a nucleation and growth process or a massive transformation, as suggested by recent electron microscopy observations and kinetic analysis. The high density of lattice defects within the τ-phase that develops during the phase transformation is attributed to growth faults produced during atomic attachment at the migrating interface. Practically, the tetragonal τ phase, which is metastable, is usually produced either by a rapid quenching of the high temperature ϵ phase followed by isothermal annealing between 400° C. and 700° C., or by cooling the ϵ phase at a rate of ~10° C./min. Prolonged annealing and elevated temperatures result in decomposition of the τ phase into the equilibrium cubic γ_2 and β phases (see FIG. **20**).

[0084] In order to stabilize the τ-phase, carbon has been introduced into Mn—Al. Carbon reduces the Curie temperature T_C, and the magnetic anisotropy field, but increases M_S with a larger resultant Mn moment. It should be pointed out that Mn—Al—C magnets have a very low Curie temperature T_C of ~290-300° C., compared with ~700-800° C. for Alnico and ~450° C. for ferrite. The workability is also improved due to the small C atoms that relieve internal lattice stresses. In $Mn_{53.6}Al_{44.6}$ alloys, the best magnetic properties were obtained for a carbon content just above the solubility limit of

carbon atoms (1.7 atomic %) because of the formation of non-magnetic Mn_3AlC precipitates. The magnetic hysteresis behavior of Mn—Al—C is extremely sensitive to the microstructure and defects introduced during the formation of the τ phase within the high temperature ϵ phase. So far, useful permanent magnets have been obtained only by doping the alloy with carbon and extruding them. Anisotropic Mn—Al—C magnets have been produced by subjecting the ternary alloys to warm extrusion. The properties of the extruded material are a result of the high anisotropy, grain size reduction and carbide precipitations.

[0085] It is desirable that the resulting bulk material is able to be machined for engineering applications. In order to determine the utility of the material for this purpose and determine its structural integrity, tensile tests may be performed at 1×10^{-4} s^{-1} in air on specimens from the ECAE-processed rods after different extrusions to determine their yield strengths and elongation at room temperature. The fracture surfaces may be examined in the SEM. Their behavior will be compared to that of the non-nanocrystalline MnAl. Additionally, correlating the magnetic properties and phase transformations with the microstructure via modeling help understand the magnetic behavior and further refine the processing and alloy compositions. Modeling that relates the observed phases to the temperature and time at temperature as well as the extrusion pressures may be used to guide the processing to obtain the optimum conditions. software Thermo-Calc and DICTRA may be used to model the phase transformations.

[0086] The above description of the specific embodiments may be modified and/or adapted for various applications or uses that do not depart from the general scope hereof. Therefore, such adaptations and modifications should and are intended to be comprehended within the meaning and range of equivalents of the disclosed embodiments. It is to be understood that the phraseology or terminology employed herein is for the purpose of description and not limitation.

[0087] This specification contains numerous citations to references such as patents, patent applications, and publications. Each is hereby incorporated by reference.

What is claimed is:

1. A bulky consolidated nanostructured manganese aluminum alloy comprising at least about 80% of a magnetic τ phase and having a macroscopic composition of $Mn_XAl_YDo_Z$, wherein

Do is a dopant,

X ranges from 52-58 atomic %,

Y ranges from 42-48 atomic %, and

Z ranges from 0 to 3 atomic %.

2. The bulky consolidated nanostructured manganese aluminum alloy of claim **1**, wherein the manganese aluminum alloy further comprising carbon having a macroscopic composition of 51 atomic % manganese, 46 atomic % aluminum and 3 atomic % carbon.

3. The bulky consolidated nanostructured manganese aluminum alloy of claim **2**, wherein the permanent magnetic properties comprise coercive forces of about 5.2 kOe.

4. The bulky consolidated nanostructured manganese aluminum alloy of claim **1**, wherein the manganese aluminum alloy has a macroscopic composition of 54 atomic % manganese, 46 atomic % aluminum.

5. The bulky consolidated nanostructured manganese aluminum alloy of claim **4**, wherein the permanent magnetic properties comprise coercive forces of about 4.8 kOe.

6. A method for producing a bulky nanocrystalline solid comprising

melting a mixture of metals comprising between 52-58 atomic % manganese and between 42-48 atomic % aluminum to form a substantially homogenous solution;

casting the solution to form ingots;

measuring compositions of the ingots;

crushing the ingots to form crushed powders;

milling the crushed powders to form nanocrystalline powders;

verifying the presence of τ phase and determining the amount of the τ phase; and

simultaneously consolidating the nanocrystalline powders into a bulky nanocrystalline solid and undergoing phase transformation from ϵ phase to at least 80% τ phase, β and γ_2 phases.

7. The method of claim **6**, further comprising characterizing microstructure of the bulky nanocrystalline solid and measuring magnetic properties of the bulky nanocrystalline solid.

8. The method of claim **6**, further comprising annealing the nanocrystalline powders to determine conditions for consolidating the nanocrystalline powders.

9. The method of claim **8**, further comprising annealing at temperatures between 200° C. and 600° C. to maximize the amount of the magnetic metastable τ phase transformed from a milled nanocrystalline unstable high-temperature ϵ phase, thereby minimizing the presence of non-magnetic equilibrium β and γ_2 phases.

10. The method of claim **8**, wherein the annealing time is shorten for higher annealing temperature to avoid decomposition of the τ-phase into the γ_2 and β phases.

11. The method of claim **6**, the step of consolidating the milled powders comprising backpressure assisted Equal channel angular extrusion (ECAE).

12. The method of claim **11**, further comprising increasing backpressure to consolidate the nanocrystalline powders.

13. The method of claim **11**, further comprising controlling a temperature of the nanocrystalline powders within 200° C. to 600° C. during the ECAE.

14. The method of claim **11**, further comprising decreasing rate of extrusion with increasing temperature to shorten annealing time at higher temperature to avoid decomposition of the τ-phase into the γ_2 and β phases.

15. The method of claim **11**, wherein the bulky nanocrystalline solid is in a form of rod shapes.

16. The method of claim **15**, wherein the bulky nanocrystalline solid has a cross-section in one of square, rectangular, and circular shape.

17. The method of claim **6**, further comprising repeating the step of consolidating the nanocrystalline powders until the bulky nanocrystalline solid having minimum defects.

18. The method of claim **6**, wherein the bulky nanocrystalline solid is machinable.

19. The method of claim **6**, wherein the mixture of metals further comprises a dopant comprising at least one of carbon and boron.

20. The method of claim **6**, wherein the mixture of metals comprises 54 atomic % manganese, and 46 atomic % aluminum.

21. The method of claim **6**, wherein the mixture of metals comprises 51 atomic % manganese, 46 atomic % aluminum and 3 atomic % carbon.

* * * * *